GeroScience
https://doi.org/10.1007/s11357-026-02119-9

ORIGINAL ARTICLE

Novel multi-omic biomarkers to combat oocyte and ovarian aging

Pawel Kordowitzki · Shakchhi Joshi · Xutong Gong · Albert Kejun Ying · Jakub Wyroba · Joanna Kochan · Marcia C. Haigis

Received: 5 November 2025 / Accepted: 21 January 2026

Abstract Understanding oocyte and ovarian aging has become critically important, as trends in family planning evolve, with many women choosing to have children later in life. The ovary, a crucial organ in female reproduction, is particularly susceptible to age-related changes and is one of the organs that exhibit functional deterioration most distinctly with age. The aging of female reproductive systems also affects longevity and various health outcomes. A better understanding of both oocyte and ovarian aging will lay the cornerstone to elucidate the phenomenon of longevity in women. Here, clinical data from 400 women of various ages undergoing intracytoplasmic sperm injection (ICSI) have been analyzed, including Anti-Müllerian Hormone (AMH) and Follicle-Stimulating Hormone (FSH) levels, the number of recovered oocytes, blastocyst rates, pregnancy rates, and live birth rates. Our analyses revealed significant differences in the aforementioned rates between patients of young and advanced age. For the biomarker analysis, we further utilised a novel predictive performance of age-associated gene expression signatures for oocyte aging, demonstrating its potential to provide molecular-level insights into oocyte quality over time. By analyzing RNA sequencing data generated from human oocytes of different ages, a genome-wide landscape of age-associated gene expression has been described. Additionally, metabolome profiling has been performed on young and reproductively aged mice, serving as a model for human ovaries. Changes in metabolites of the murine ovaries during aging have been recorded. In conjunction with traditional biomarkers, multiomics data represent a

P. Kordowitzki (✉)
Department of Basic and Preclinical Sciences, Nicolaus Copernicus University, Torun, Poland
e-mail: paul.kordowitzki@charite.de

P. Kordowitzki · S. Joshi · X. Gong · M. C. Haigis
Department of Cell Biology, Blavatnik Institute, Harvard Medical School, Boston, USA

P. Kordowitzki
Department of Gynecology, European Competence Center for Ovarian Cancer, Charité, University Medicine Berlin, Augustenburgerplatz 1, Berlin, Germany

X. Gong
Department of Immunology, Blavatnik Institute, Harvard Medical School, Boston, USA

A. K. Ying
T. H. Chan School of Public Health, Harvard University, Boston, USA

J. Wyroba · J. Kochan
Malopolski Institute of Fertility Diagnostics and Treatment – KrakOvi, Krakow, Poland

J. Wyroba
Fertility Disorders Clinic, Andrzej Frycz Modrzewski Krakow University, Krakow, Poland

Published online: 03 February 2026

transformative approach in reproductive health, and they may offer personalised risk assessments and interventions to mitigate age-related fertility decline in women. Our metabolome profiling provides a valuable resource for elucidating the metabolomic basis of ovarian aging. Our findings offer novel insights into systemic shifts associated with oocyte and ovarian aging. This integrated approach may unlock new avenues for fertility preservation, ovarian rejuvenation, and assisted reproduction.

Keywords Oocyte · Ovary · Blastocyst · Aging · Metabolome · Metabolite · Biomarker · RNA sequencing · Women

Introduction

Recent socio-economic changes have led to a delay in parenthood, aligning with the global reduction in fertility rates and population growth [1–5]. Understanding oocyte and ovarian aging has become critically important, as trends in family planning evolve, with many women choosing to have children later in life. This phenomenon, particularly evident in developed countries, appears to be irreversible, culminating in a demographic shift toward an older population and a corresponding decline in population growth [5]. Additionally, lifestyle modifications and diet have impacted the fertility outcomes of the twenty-first century. Factors such as obesity, reflected by the body mass index, negatively affect female fertility and reduce the chances of successful assisted reproductive technologies (ART) in women. As a result, there is an urgent requirement to enhance human fertility [2, 6]. The ovary, an essential organ in female reproduction, is particularly susceptible to age-related alterations and is one of the organs most distinctly exhibiting functional deterioration with age [7, 8]. The aging of female reproductive systems also affects longevity and various health outcomes [9–11].

The pursuit of understanding biomarkers for oocyte and ovarian aging has garnered considerable attention in the realm of reproductive medicine. These biomarkers offer critical insights into ovarian physiology and viability as women age, presenting substantial implications for fertility treatments and reproductive health strategies. In this regard, RNA sequencing and metabolic profiling represent an emerging and promising approach to identifying biochemical markers of ovarian aging. Metabolites serve as indicators of physiological changes associated with aging. They reflect the dynamic biochemical processes influenced by genetic, environmental, and lifestyle factors. Recent research has identified specific metabolites that correlate with age-related decline in health. Metabolites related to energy production, amino acid metabolism, and oxidative stress pathways serve as indicators of ovarian health [12, 13]. For example, the levels of metabolites like lactate and pyruvate can reflect the efficiency of glycolysis and oxidative phosphorylation, respectively [14]. Metabolic profiling thus offers a comprehensive view of the biochemical status of the ovary, aiding in the assessment of its viability during aging. Moreover, biomarkers such as lipid peroxidation products and antioxidant enzyme activities serve as valuable indicators of oxidative stress within the ovary [15–19]. Variations in these lipid components have been linked to the pathology of numerous aging-related diseases, emphasizing the importance of understanding their biochemical interactions [20–25].

To date, hormonal indicators have been widely utilized as reliable markers of ovarian reserve. The Follicle-stimulating hormone (FSH) and anti-Müllerian hormone (AMH) are particularly prominent in this regard [2, 26]. With advancing age, elevated levels of FSH often indicate a diminished ovarian reserve, reflecting a reduced pool of viable oocytes. Conversely, lower AMH levels correlate with lower antral follicle counts, serving as an early sign of declining ovarian function. Both FSH and AMH are integral to predicting ovarian response in fertility treatments, emphasizing their roles as crucial physiological biomarkers [27, 28]. Integrating metabolomics with other omics technologies can enhance our comprehension of aging pathways. However, the metabolites relevant to the aging phenomenon in ovaries remain elusive. Ovarian aging is driven by innate biological mechanisms and cumulative environmental stressors, resulting in reduced fertility. Leveraging these discoveries, novel approaches such as metabolomics, transcriptomics, telomere length, and biological clocks are emerging as powerful tools to precisely quantify oocyte and ovarian aging.

This being said, several key questions anchor this investigation: What are the reliable, non-invasive biomarkers that can accurately assess oocyte and ovarian aging? What are the practical applications of these biomarkers in contemporary fertility treatments? To

answer these questions, we analyzed the clinical data of 400 women of different ages undergoing intracytoplasmic sperm injection, including AMH and FSH levels, recovered oocyte numbers, blastocyst rates, pregnancy rates, and the live birth rate. We utilized a novel predictive performance of age-associated gene expression signatures for oocyte aging, demonstrating its potential to provide molecular-level insights into oocyte quality over time. By analyzing RNA sequencing data generated from human oocytes of different ages, we further identified a genome-wide landscape of age-associated gene expression. Moreover, metabolome profiling in murine ovaries of different ages has been performed to describe a novel metabolomic-based biomarker for ovarian aging. Our findings offer novel insights into shifts associated with oocyte and ovarian aging. This integrated approach may unlock new avenues for fertility preservation, ovarian rejuvenation, and assisted reproduction.

Materials and methods

Patient data

This was a retrospective study of 400 women who underwent only intracytoplasmic sperm injection (ICSI) cycles at a Krakovi Clinic in Kraków (Poland) from 2021 to 2024. The ICSI procedure is predominantly chosen in this clinic; therefore, conventional in vitro fertilization (IVF) has not been considered. We have analyzed two groups of patients, young (below the age of 35 years) and advanced age patients (above 35 years of age). The patients' age range was from 26 to 44 years. Institutional ethics committee approval (KBKA/07/O/2024) was obtained.

Inclusion criteria

Based on the diagnostic criteria for intracytoplasmic sperm injection, the inclusion criteria of patients enrolled in this study need to satisfy at least two of the following three criteria 3: (1) AMH > 0.5 ng/mL; (2) AFC > 2 follicles; and (3) bFSH ≥ 10 IU/L.

Exclusion criteria

Patients with any of the following conditions were excluded: (1) polycystic ovary or polycystic ovary syndrome; (2) chronic diseases, such as hypertension, cardiovascular disease, autoimmune disease, and abnormal hepatic and renal function; (3) other endocrine diseases, such as hypogonadotropin hypogonadism (HH) and hyperprolactinemia; (4) uterine malformation; (5) chromosome abnormality; (6) a history of recurrent spontaneous abortion; and (7) an active period of infectious diseases.

Clinical protocols

Patients were treated using either the long agonist protocol or the short antagonist protocol. The type of protocol used depended on the AMH level and the overall hyperstimulation risk.

Long agonist protocol

Starting 1 week before the expected menses (cycle day 18−23), patients received the GnRH agonist, triptorelin (Decapeptyl, 1 mg/d, sc). After successful pituitary downregulation (when the serum estradiol (E2) levels were < 40 pg/mL), ovarian stimulation was commenced with a fixed daily dose of 150–300 IU recombinant follitropin alfa (rFSH, sc) with or without an additional 75−150 IU menotropin (hMG).

Antagonist protocol

A GnRH antagonist Cetrorelix (Cetrotide, 0.25 mg/d, sc) or Ganirelix (0.25 mg/d), was administered, commencing when the largest follicle reached a diameter of 14 mm. rFSH/hMG was initiated on day 2–4 of the cycle. The agonist and antagonist protocols were continued up to and including the day of human chorionic gonadotropin (hCG) administration, which was when the leading follicle reached a diameter of 18 mm or more and at least three follicles reached a diameter of 17 mm or more. rFSH was then stopped, and a single sc bolus of 10,000 IU hCG (Eutrig) or 6500 IU rhCG (Ovitrelle) was administered 36 h before the planned time of oocyte retrieval. When there was a risk of OHSS in an antagonist cycle, the trigger was a single sc bolus of triptorelin 2 mg, and a freeze-all policy was applied. All follicles 12 mm or larger were aspirated. Subsequently, the oocytes were inseminated via ICSI, and a single embryo was transferred 3 or 5 days later. Luteal support in the form of intravaginal progesterone (Cyclogest, 400 mg twice

a day) was administered starting from the day after oocyte retrieval until a serum pregnancy (b-hCG) test was performed 17 days later.

Ovarian stimulation monitoring in ICSI

Baseline blood sampling and transvaginal sonography (TVS) was performed on day 2 or 3 of the pretreatment cycle for all patients. Monitoring of responses during the treatment cycle consisted of TVS and blood sampling for hormonal analysis on cycle days 2–3 (E2, FSH, LH); 5–6 (E2); 8–9 (E2); and the day of hCG administration (E2, P4). Additional TVS monitoring was performed as clinically indicated.

Preparation for frozen embryo transfer

Treatment with oral E_2 was started on the first, second, or third day of the cycle to prime the endometrium and suppress spontaneous follicle growth. Oral estradiol was administered in an incremental fashion: 2 mg/day during days 1–7, 4 mg/day during days 8–12, and 6 mg/day during days 13 to embryo transfer. Usually, after 12–14 days of E2 administration, vaginal ultrasound examination was performed for endometrial thickness measurement and to confirm the absence of a dominant follicle. When the endometrial thickness was greater than 7 mm, P4 supplementation was initiated, and the timing of FET was scheduled accordingly. For t-NC, TVS was performed on day 2 or 3 of menses to rule out any cyst or *corpus luteum* remaining from the previous cycle. Cycle cancellation was typically undertaken in cycles with serum P4 levels greater than 1.5 ng/ml on days 2 or 3 of menses. Transvaginal ultrasonographic monitoring was usually started on day 8–10, and endocrine monitoring, measuring serum E2, LH, and P4, was performed when the leading follicle attained a mean diameter of approximately 15 mm. Following frequent endocrine and ultrasonographic monitoring, on alternate days or daily, the day of ovulation was precisely documented to schedule the timing of FET.

Laboratory protocols

ICSI was performed using a Nikon Eclipse CS100 microscope and an RI Integra 3 micromanipulator (Research Instruments, Germany), following the standard technique. Embryos were in vitro cultured in SAGE® medium (Origio, Denmark) in an atmosphere of 6.0% CO_2, 5.0% O_2, and balanced N_2 at 37 °C. Blastocysts were graded according to the Gardner scoring criteria based on the degree of expansion, as well as inner cell mass (ICM) and TE morphology. In cases where the patient was not adequately synchronized for a direct fresh embryo transfer, blastocysts were vitrified using Kitazato media and the Cryotop device (Kitazato, Japan) according to the manufacturer's protocol. Blastocysts were warmed in Kitazato media for a minimum of 1.5 h before transfer and then placed in EmbryoGlue medium (Vitrolife, Sweden) or in Sage medium. More than 95% of transfers were performed in Embryo Glue® medium.

Mouse handling and care

All procedures performed on mice were carried out in accordance with the relevant guidelines: EU Directive of the European Parliament and the Council on the protection of animals used for scientific purposes (22 September 2010; No 2010/63/EU), Polish Parliament Act on Animal Protection (21 August 1997, Dz.U. 1997 nr 111 poz. 724) with further novelization—Polish Parliament Act on the protection of animals used for scientific or educational purposes (15 January 2015, Dz.U. 2015 poz. 266). The experimental procedures were approved by the Local Ethics Committee for Experiments on Animals of the Harvard Medical School Standing Committee on Animals and the National Institutes of Health. All mouse protocols were approved by the Harvard Medical Area Standing Committee on Animals. Procedures were performed with 28 female mice (with MDX PHD3 CMV background) at the ages of six months ($n = 14$) and 12 months ($n = 14$). Mice were sacrificed using cervical dislocation. The mice for metabolic profiling were obtained from The Jackson Laboratory and housed in the New Research Building Animal Facility at Harvard Medical School. Mice were housed at 20–22 °C on a 12 h light/dark cycle with ad libitum access to food (LabDiet 5053) and water.

Metabolite profiling and mass spectrometry

Metabolites were extracted from flash-frozen ovarian tissue (approximately 5 mg per sample) using 1 mL of pre-chilled extraction solvent (2:2:1 [v/v/v] acetonitrile:methanol:water, at –20 °C). The tissue

homogenate was vigorously vortexed for 15 min at 4 °C, then centrifuged at 16,000 × g for 15 min (4 °C). The resulting supernatant was collected and concentrated to dryness in a refrigerated vacuum evaporator. The dried extract was reconstituted in 1:1 acetonitrile:water (volume normalized to tissue weight) for subsequent LC–MS analysis.

Chromatographic separation was performed on a Thermo Fisher Vanquish ultrahigh-performance liquid chromatography (UHPLC) system using hydrophilic interaction liquid chromatography (HILIC). An iHILIC-(P) Classic column (150 mm × 2.1 mm, 5 µm particle size, 200 Å pore) with a matching guard column was maintained at 25 °C (with a 30 °C pre-column heater). The mobile phase consisted of 20 mM ammonium carbonate with 0.1% ammonium hydroxide in water (buffer A) and acetonitrile (buffer B). The flow rate was 0.15 mL/min. A linear gradient was applied from 95% B at 0 min to 5% B at 23 min, held at 5% B until 25 min, then increased back to 95% B by 25.5 min (with a brief flow ramp to 0.20 mL/min for column washing) and re-equilibrated at 95% B until 33 min.

The UHPLC was coupled to a high-resolution Q Exactive HF-X Hybrid Quadrupole-Orbitrap mass spectrometer (Thermo Fisher Scientific) equipped with a heated electrospray ionization (HESI) source operating in negative ion mode. Mass spectra were acquired in full-scan mode from *m/z* 70–1000 at 60,000 resolving power (at *m/z* 200). An automatic gain control target of 1 × 10^5 ions and a maximum injection time of 20 ms were used, with in-source collision-induced dissociation set to 5 eV. The electrospray source parameters were: spray voltage 3.0 kV; capillary temperature 275 °C; probe heater 350 °C; sheath gas 40, auxiliary gas 15, and sweep gas 1 (arbitrary units).

Data acquisition and peak integration were performed using Thermo TraceFinder v4.1. Metabolites were identified by matching the observed retention times and exact masses (within 5 ppm tolerance) to an in-house library of authentic standards. Detected peaks were manually curated to remove noise or inconsistent signals. A deuterated internal standard (D8-phenylalanine) was spiked into each sample prior to extraction to monitor recovery and instrument drift. All metabolite intensities were normalized to the internal standard and to tissue input amount for quantitative comparisons. Downstream statistical analyses (univariate testing and pathway enrichment) were carried out using MetaboAnalyst 6.0, with additional data visualization and significance testing performed in GraphPad Prism.

Metabolite profiling data processing

All raw LC–MS data files were converted to an open format using ProteoWizard (v3.0.8789). We then utilized the XCMS R package (v3.1.3) [29–31] for untargeted feature detection, retention-time alignment, and peak integration across samples. This processing pipeline generated a matrix of features characterized by their mass-to-charge ratio (m/z), retention time, and peak area. In total, approximately 14,881 ion features were detected in positive ionization mode and ~ 11,947 in negative mode across the ovarian samples. The aligned feature table was exported for analysis in MetaboAnalystR [29–31]. Prior to statistical analysis, intensity values were log-transformed and normalized to the internal standard and sample mass to minimize technical variability.

Smart-seq2 libraries and gene expression analysis

Herein, data from paired-end Smart-seq2 sequencing on human metaphase II oocytes from previously published studies, which are publicly available [32–39], are used. These studies were sourced from both a recent systematic review of human oocyte transcriptomes [40] and the reproGenomics database [41].

Identification of age-associated genes

To identify genes whose expression levels correlate with maternal age, we performed Pearson correlation analysis between gene expression values and chronological age across all samples. Genes were ranked by their correlation coefficients, and statistical significance was determined using a two-tailed *t*-test. Multiple testing correction was applied using the Benjamini–Hochberg false discovery rate (FDR) method, with significance defined as FDR < 0.05. The top 20 age-associated genes (10 positively correlated and 10 negatively correlated) were selected for further analysis.

Gene ontology enrichment analysis

Protein-coding genes from the top 20 age-associated genes were subjected to gene ontology (GO) enrichment analysis to identify overrepresented biological processes. Non-coding RNAs (including microRNAs and small nuclear RNAs) were excluded from this analysis. GO enrichment was performed using g: Profiler (version 2024) with the following parameters: organism = *Homo sapiens*, sources = GO Biological Process (GO:BP), significance threshold method = FDR, user threshold = 0.05. GO terms with a minimum of 2 genes and FDR < 0.05 were considered significantly enriched.

Predictive modeling

To assess the utility of age-associated genes for predicting oocyte age, we constructed machine learning models using the top age-associated gene expression profiles as features. Models were trained using supervised learning approaches with cross-validation to prevent overfitting. Model performance was evaluated using standard regression metrics, including R^2, mean absolute error (MAE), and root mean square error (RMSE).

Data visualization

All visualizations were generated using Python 3.10 with matplotlib (v3.8.0), seaborn (v0.13.0), and aquarel (v0.0.5) for publication-quality styling. Age distribution plots were created as kernel density estimates. Gene expression distributions were visualized as violin plots with overlaid box plots. Volcano plots displayed effect sizes (correlation coefficients) against statistical significance ($-\log_{10}$ *p*-values). Hierarchical clustering heatmaps were generated using the Euclidean distance and average linkage methods. GO enrichment results were visualized as horizontal bar plots showing $-\log_{10}$ transformed *p*-values with gene counts annotated. Gene-pathway relationships were displayed as chord diagrams using HoloViews (v1.18.0) with Bokeh backend, connecting genes to their associated GO terms in a circular layout.

Statistical analysis

The Kolmogorov–Smirnov test (K-S test) was used to estimate the normality of the distribution. Normally distributed continuous variables were presented as means ± standard deviations (SDs), and Student's *t*-test was used to compare the statistical difference between the two groups. Non-normally distributed numerical variables were presented as medians (25th to 75th percentiles), and a nonparametric test was used to compare the statistical differences between the two groups. Two-sided *p*-values < 0.05 were considered statistically significant. Non-parametric data, such as differences in specific values between the patient groups, were assessed using either the Mann–Whitney test or the Kruskal–Wallis test, followed by a Dunn's multiple comparisons test, as we did not assume a specific distribution of the variables measured on nominal and ordinal scales. Parametric data were expressed as means ± SD and compared by two-way ANOVA. Differences were considered significant when the *p*-value was ≤ 0.05. The statistical analysis was performed using the R software, version 4.4.1 (R Project for Statistical Computing). All statistical analyses regarding gene expression data were performed in Python 3.10 using SciPy (v1.11.0), NumPy (v1.24.0), and pandas (v2.0.0). Pearson correlation coefficients were used to quantify linear relationships between gene expression and age. Two-tailed *t*-tests were used for hypothesis testing. Multiple testing correction employed the Benjamini–Hochberg FDR method. Statistical significance was defined as $p < 0.05$ or FDR < 0.05, where applicable.

Results

Developmental competence of human oocytes

The aging process profoundly influences women's reproductive health and fertility, driven by significant physiological transformations. This study rigorously investigated the critical impact of advanced maternal age on the developmental competence of oocytes (Fig. 1A). To address this, we analyzed the oocyte and blastocyst numbers from young patients in two groups: those under 35 years of age and those over 35 years of age, who underwent ICSI procedures and associated hormonal treatments, as detailed in our protocols. As can be seen in Fig. 1B, the implantation rate and ongoing pregnancy in women of advanced maternal age were significantly ($p < 0.05$) lower compared to those

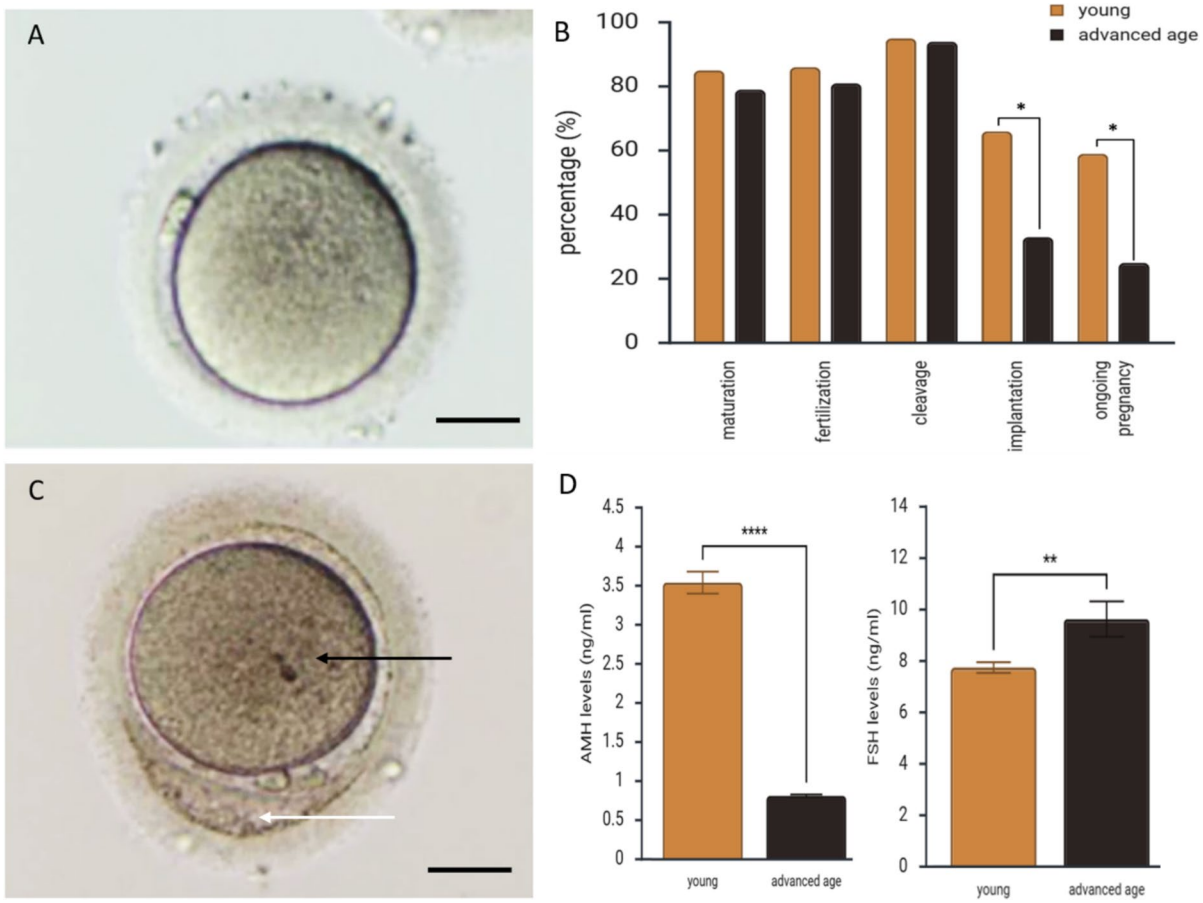

Fig. 1 Metaphase II oocytes were retrieved via ovum pick-up of young and advanced-age patients. (**A**) Representative microscopic photograph of human oocytes with proper morphology in young patients. (**B**) The Graph shows the maturation, fertilization, cleavage, blastocyst, implantation, and pregnancy rate for both age groups. (**C**) A representative microscopic photograph of improper morphology in an oocyte from patients of advanced age is shown. Here, the retrieved oocytes exhibit an increased perivitelline space (indicated by the white arrow) and irregular cytoplasm (indicated by the black arrow). The scale bar represents 20 µm. (**D**) The Graph shows the AMH and FSH levels in both age groups. Asterisks indicate statistical significance: $*=p<0.05$, $**=p<0.01$, $***=p<0.001$, $****=p<0.0001$

in women below 35 years of age. Moreover, the oocytes of women over 35 years show morphologic alterations characteristic of aged oocytes, such as an extra perivitelline space and irregular cytoplasm (Fig. 1C). The deliberate focus on this specific age group was paramount for elucidating how maternal age influences reproductive rates. Furthermore, it is essential to acknowledge that established indicators, such as serum AMH and FSH levels, serve as vital prognostic tools for predicting the expected number of oocytes and ICSI success, particularly in the context of maternal aging. The mean AMH level in the advanced maternal age group was significantly ($p<0.0001$) lower compared to the AMH levels in the young patient group, whereas for FSH, the levels were significantly ($p<0.01$) higher in the advanced age group compared to the young patient group (Fig. 1D).

Gene expression results for human oocytes of different ages

To elucidate the biological significance of age-associated genes identified in oocytes, we performed

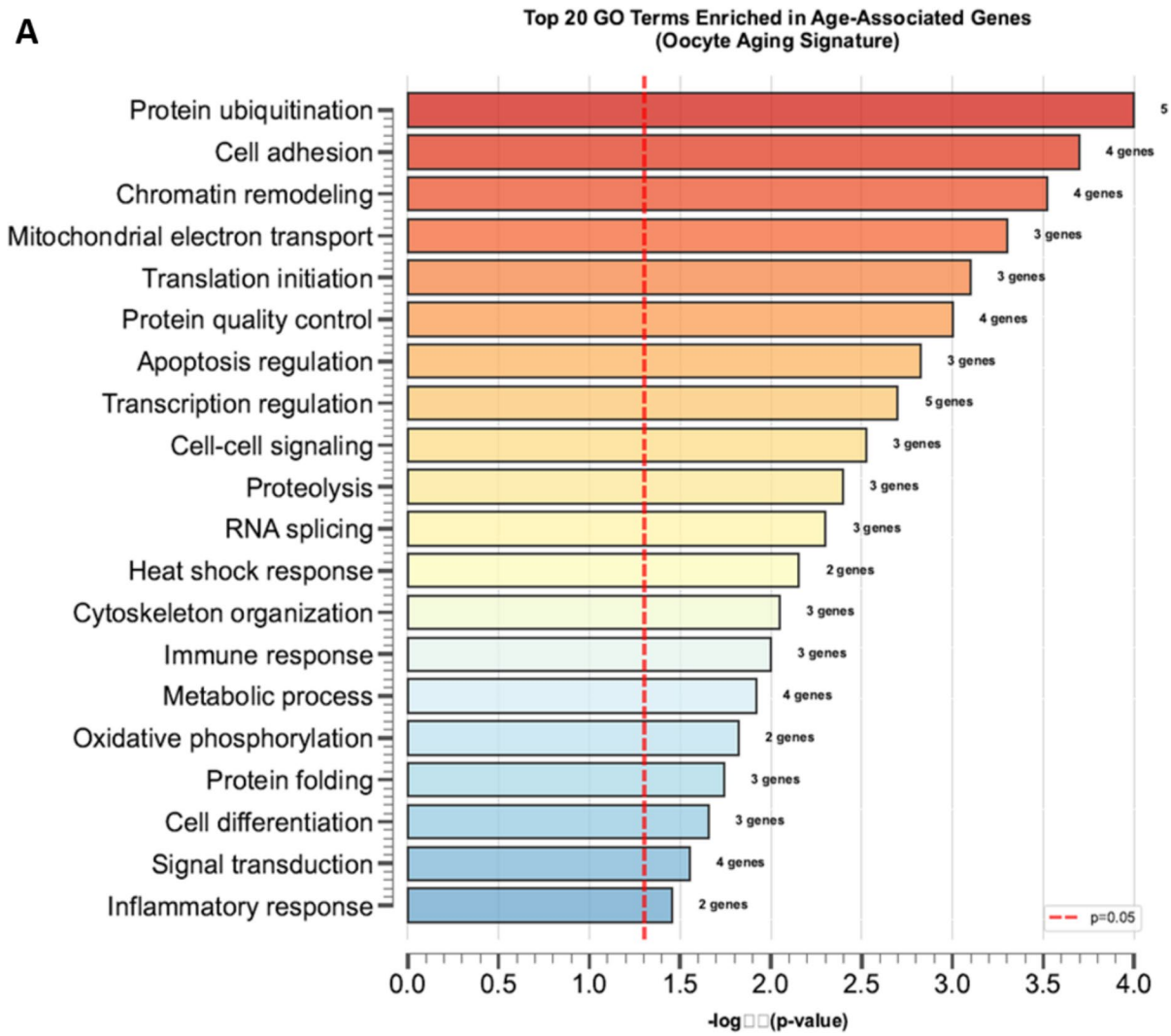

Fig. 2 Gene ontology enrichment analysis reveals key biological processes affected by oocyte aging. (**A**)Horizontal bar plot displaying the top 20 significantly enriched GO Biological Process terms among the age-associated protein-coding genes ($n = 17$). Bars represent -$\log_{10}$ transformed p-values (Fisher's exact test with FDR correction), with longer bars indicating higher significance. The red dashed line marks the significance threshold ($p = 0.05$, equivalent to -$\log_{10}$ $p \approx 1.3$). Gene counts for each pathway are annotated on the right side of each bar. The color gradient indicates the degree of enrichment significance, ranging from yellow (less significant) to red (highly significant). The enrichment analysis reveals five major biological themes: protein quality control (including protein ubiquitination, quality control, folding, and heat shock response; ~ 40% of terms), cell adhesion and communication (cell adhesion, cell–cell signaling; ~ 15%), chromatin organization and transcription (chromatin remodeling, transcription regulation, RNA splicing; ~ 20%), mitochondrial function (electron transport, oxidative phosphorylation; ~ 10%), and stress responses (apoptosis, immune response, inflammation; ~ 15%). (B) Circular chord diagram illustrating gene-pathway relationships. Genes are positioned on the upper arc (blue nodes, $n = 15$ protein-coding genes) and GO terms on the lower arc (colored nodes representing the top 10 enriched pathways). Gray ribbons connect genes to their annotated GO terms, with ribbon width proportional to the strength of association. Highly connected genes (e.g., HERC5, VCAM1, SMARCA4) exhibit pleiotropic effects, participating in multiple biological processes

Gene Ontology enrichment analysis. This analysis revealed a spectrum of biological processes significantly ($p \leq 0.05$) impacted by oocyte aging (Fig. 2A). The top 20 significantly enriched GO Biological Process terms (among 17 age-associated protein-coding genes) highlighted five major biological themes

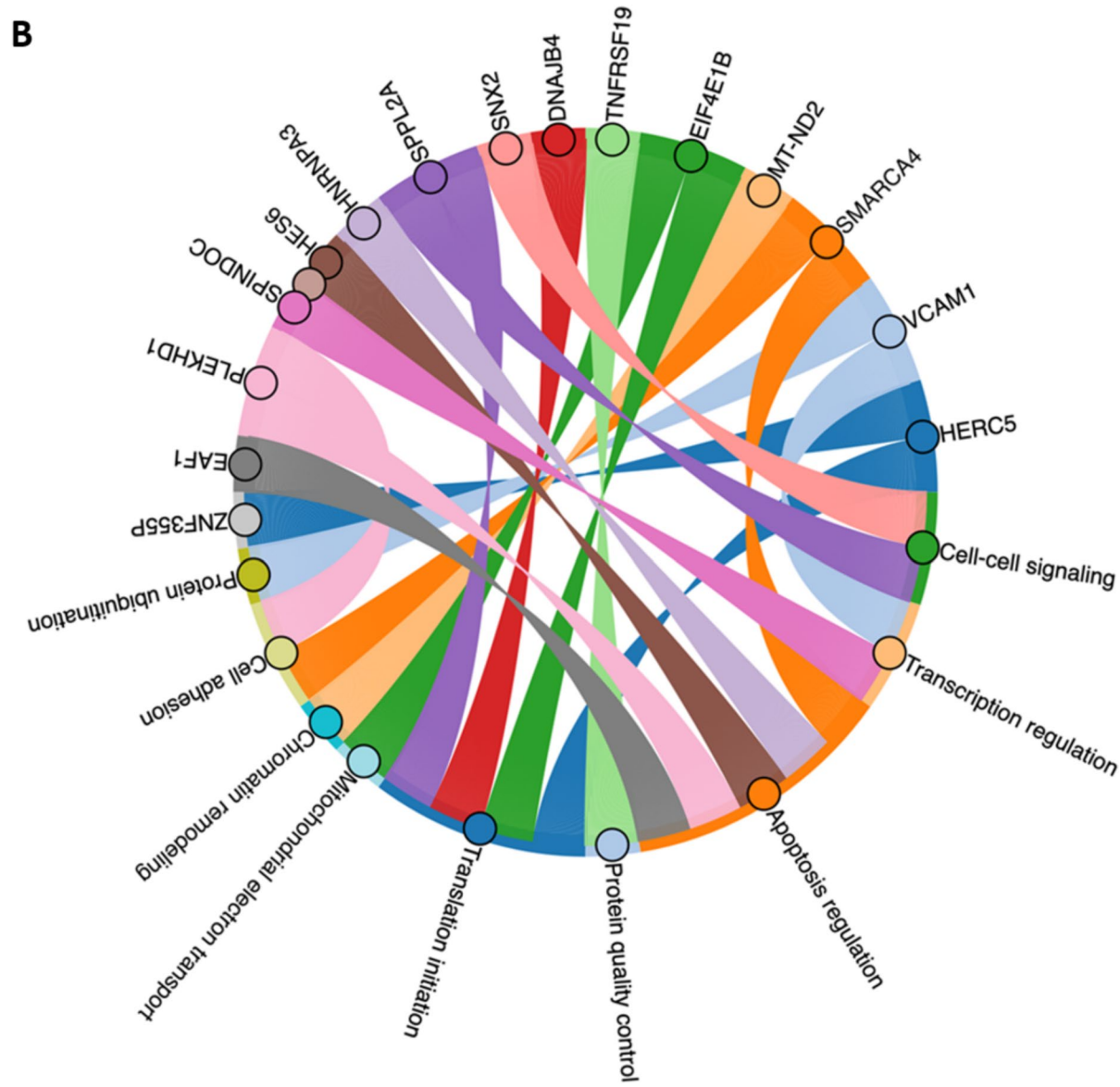

Fig. 2 (continued)

collectively contributing to oocyte aging: protein ubiquitination, protein quality control, protein folding, and heat shock response. Moreover, terms such as chromatin remodeling, transcription regulation, and RNA splicing accounted for 20% of the identified terms, and cell adhesion and cell–cell signaling constituted about 15% of the enriched processes (Fig. 2A). Interestingly, biological process terms related to mitochondrial function, such as electron transport and oxidative phosphorylation pathways, as well as processes related to stress responses, such as apoptosis, immune response, and inflammation pathways, were significantly ($p \leq 0.05$) enriched terms for aged oocytes. The circular chord diagram was constructed to visualize the intricate gene-pathway relationships, and illustrates 15 protein-coding genes on the upper arc and the top 10 enriched GO terms on the lower arc (Fig. 2B). This network visualization demonstrated that highly connected genes, such as *HERC5, VCAM1*, and *SMARCA4*, exhibit pleiotropic

effects, participating in multiple biological processes. Notably, protein quality control pathways received input from the largest number of age-associated genes, underscoring proteostasis decline as a central hallmark of oocyte aging. The observed gene clustering patterns suggest the existence of functional modules that undergo coordinated dysregulation during the aging process of oocytes. Besides, the top ten representative age-associated genes across the oocyte cohort, namely *VCAM1*, *HERC5*, *RNU1-1*, *SPPL2A, DNAJB4*, *TNFRSF19*, *PLEKHD1*, *MIR335, SMARCA4*, and *MT-ND2* are shown in Fig. 3A. As shown by the Kernel density plot, the distribution of maternal ages in the study cohort spans ages 20–43 years, which encompasses the critical period of reproductive aging in women, allowing for the robust identification of age-associated molecular changes (Fig. 3B).

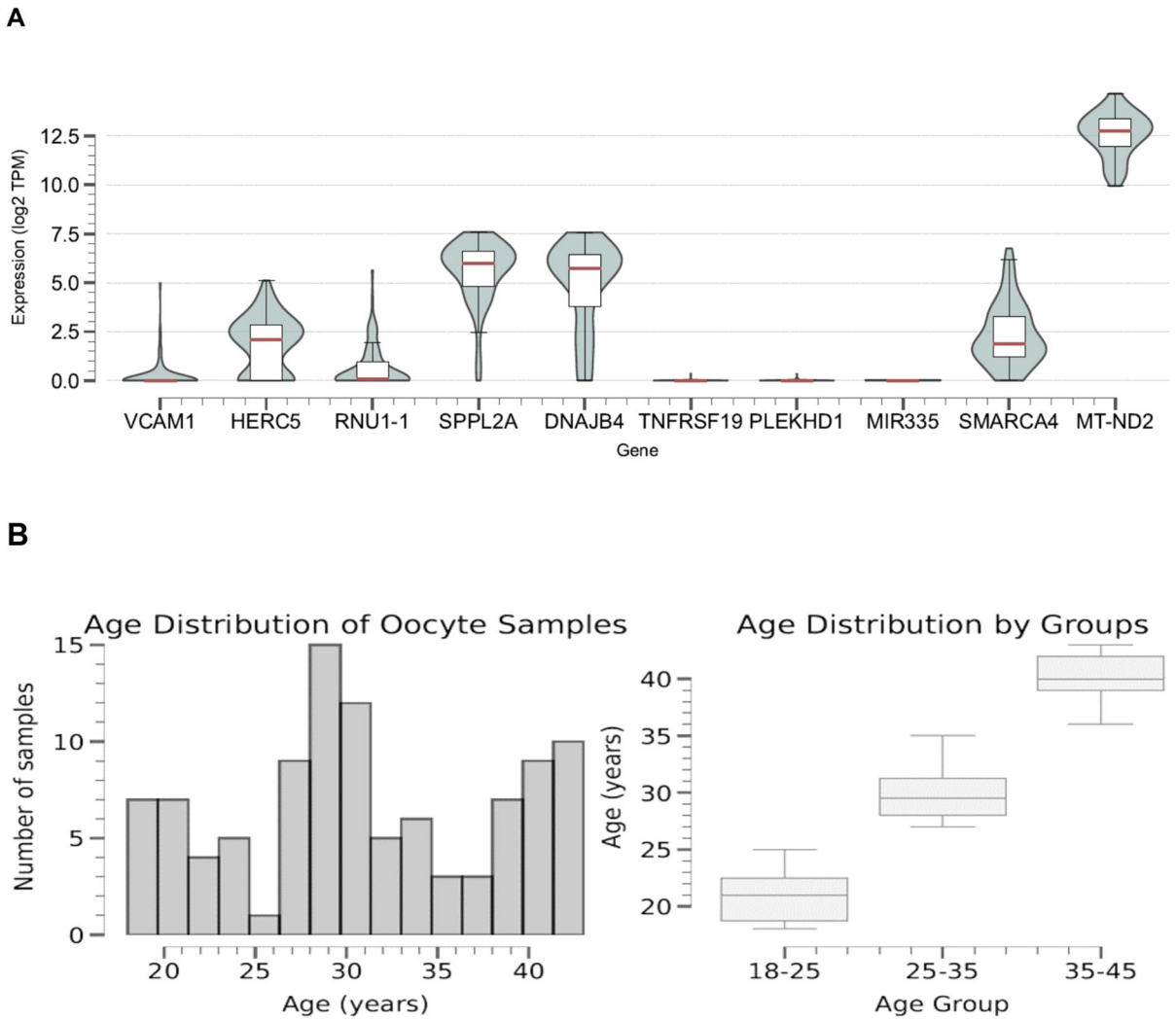

Fig. 3 Expression distributions of age-associated genes. (**A**) Violin plots depicting the expression distributions of representative age-associated genes across the oocyte cohort. Each violin represents the probability density of expression values ($\log_2$ TPM), with overlaid box plots showing median (center line), interquartile range (box), and 1.5 × interquartile range (whiskers). Genes shown include both negatively correlated and positively correlated ones, illustrating the range of expression variability and the directionality of age associations. (**B**) Kernel density plot showing the distribution of maternal ages in the study cohort. The distribution spans ages 20–43 years. This age range encompasses the critical period of reproductive decline, allowing for the robust identification of age-associated molecular changes

Aging-associated gene expression results

To identify transcriptional changes associated with maternal aging, we performed an unsupervised hierarchical clustering analysis of the top 20 age-associated genes across individual oocyte transcriptomes. The clustering analysis revealed two major gene expression patterns, as shown in the respective heatmap (Fig. 4). The first cluster comprises negatively age-correlated genes, including *HERC5*, *VCAM1*, *SPPL2A*, and *DNAJB4*, which exhibit a progressive downregulation with increasing maternal age. In contrast, the second cluster comprises positively age-correlated genes, such as *PLEKHD1, TNFRSF19, SMARCA4*, and *MT-ND2*, which exhibit a gradual upregulation in oocytes of advanced maternal age. Moreover, to characterize transcriptional signatures associated with maternal age, we assessed the correlation between gene expression levels and chronological age across all oocyte samples. The volcano plot illustrates the relationship between effect size on the x-axis and statistical significance on the y-axis (Fig. 5). Notably, genes located in the upper corners of the plot exhibit both strong correlation coefficients and high statistical significance. Among these, the top 20 age-associated genes are highlighted and labeled, displaying a clear separation from the background distribution and underscoring their robust association with maternal age (Fig. 5). Furthermore, we evaluated the predictive performance of the age-associated

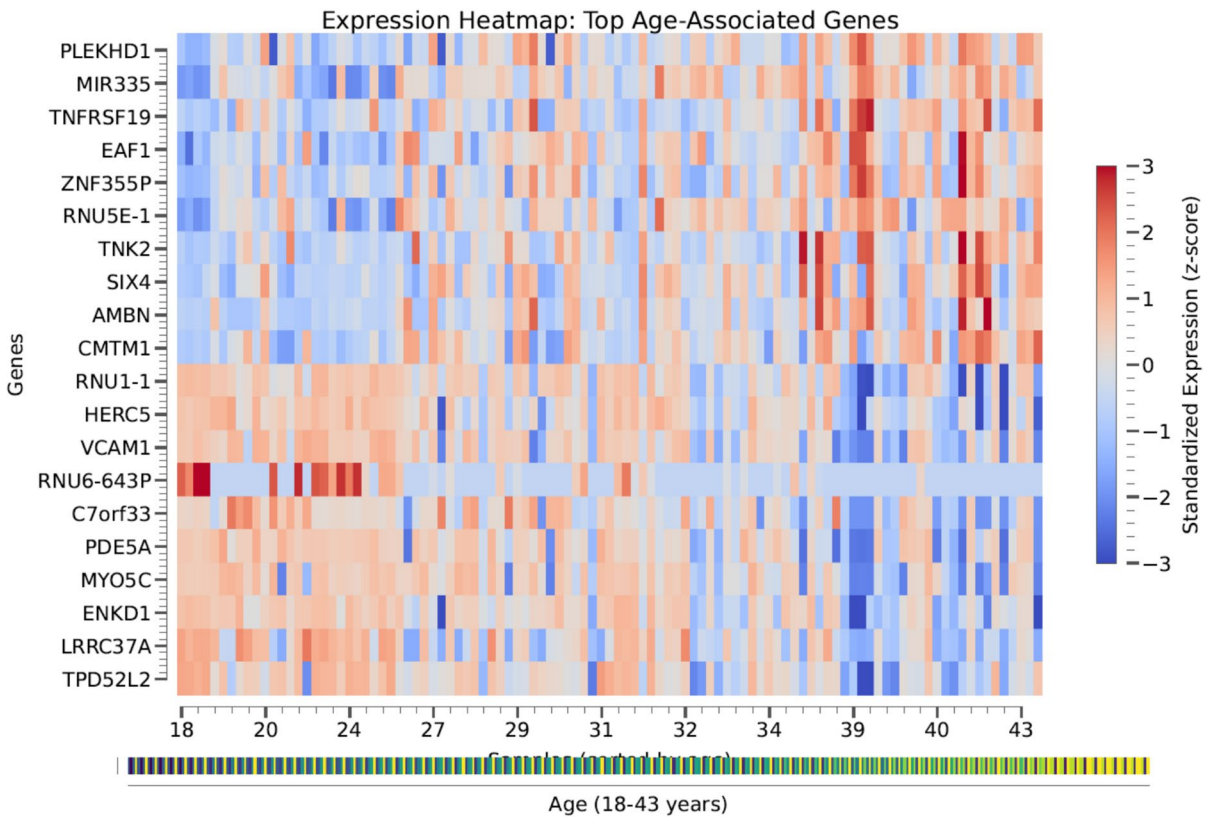

Fig. 4 Hierarchical clustering of top age-associated genes reveals distinct age-related expression patterns. Heatmap showing unsupervised hierarchical clustering of the top 20 age-associated genes (rows) across individual oocyte samples (columns). Samples are ordered by maternal age (x-axis). Gene expression values are row-normalized and displayed as z-scores, with red indicating higher expression and blue indicating lower expression relative to the mean. The heatmap reveals two major gene clusters: negatively correlated genes (HERC5, VCAM1, SPPL2A, DNAJB4, and others), which show progressive downregulation with age, and positively correlated genes (PLEKHD1, TNFRSF19, SMARCA4, MT-ND2, and others), which show upregulation with age. Hierarchical clustering was performed using the Euclidean distance and average linkage method. This pattern suggests coordinated dysregulation of multiple biological processes during oocyte aging

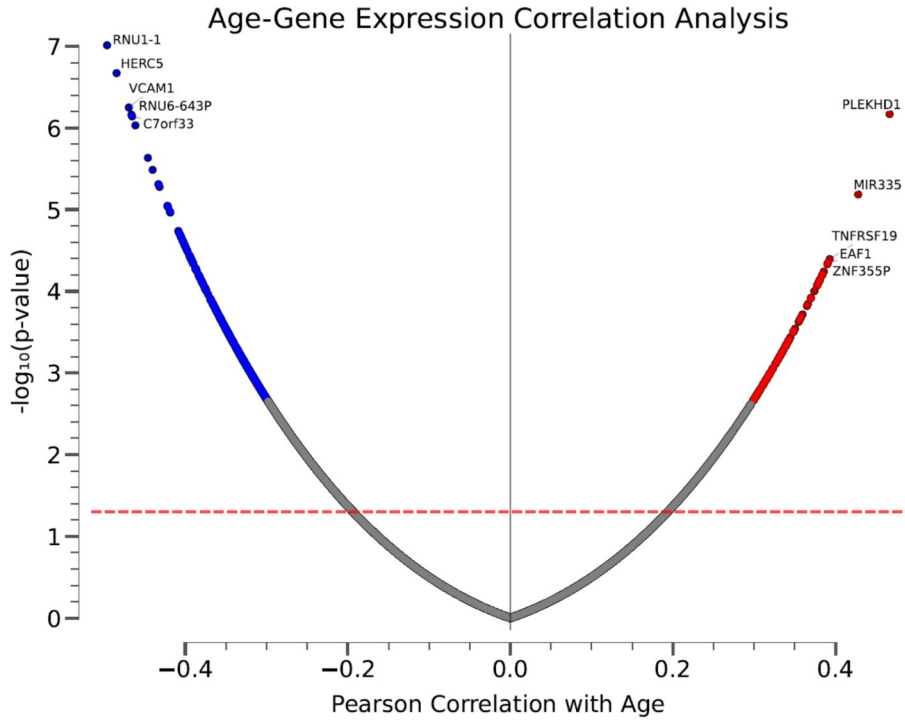

Fig. 5 Genome-wide landscape of age-associated gene expression. Volcano plot displaying the relationship between effect size (Pearson correlation coefficient, x-axis) and statistical significance ($-\log_{10}$ p-value, y-axis) for all genes analyzed. Each point represents a single gene, with color intensity indicating significance level. Genes in the upper corners represent those with both strong correlations and high statistical significance. Dashed horizontal line indicates the significance threshold ($p = 0.05$). The top 20 age-associated genes are highlighted and labeled, demonstrating clear separation from the background distribution

transcriptomic model, and the prediction accuracy was examined across the maternal age range. Figure 6 demonstrates the model prediction accuracy across age ranges, showing that the Elastic Net model captures age-related patterns reasonably well, with stronger performance in the training dataset and moderate predictive ability in the test set. The residual distributions suggest acceptable model behavior without strong systematic bias, though generalization is limited, likely due to sample size and biological variability. These analyses demonstrate that the earlier-mentioned genes exhibit strong and statistically significant correlations ($p \leq 0.05$) with maternal age, and that the developed model reliably captures age-related transcriptional changes across the reproductive lifespan. To evaluate the predictive capacity of age-associated transcriptional changes, we developed machine learning models trained on oocyte gene expression profiles correlated with maternal age, as shown in Fig. 7. The latter-mentioned figure represents a model performance comparison across Elastic Net, Ridge, linear regression, LASSO, random forest, and gradient boosting models, which were evaluated using test-set R^2 and mean absolute error. Moreover, the bar plot illustrates the feature importance for the Elastic Net model, displaying the top 20 genes ranked by absolute coefficient magnitude, and highlighting transcripts with the strongest contributions to biological age prediction in oocytes. Corresponding model performance metrics confirm the model's robust predictive accuracy across the dataset. To further explore the molecular drivers of prediction accuracy, feature importance analysis was performed (Fig. 7). These multiple machine-learning models were used to predict age and identify the most informative features, as highlighted by the best-performing model. The results demonstrate that ElasticNet provides the most robust and generalizable age prediction among the tested models. It balances predictive accuracy with interpretability, identifying a biologically meaningful set of key features that support its suitability for downstream analysis and interpretation.

Metabolite profiling

Targeted metabolomic analysis identified a total of 119 metabolites present in ovarian tissues from both young and aged mice. Differential abundance analysis pinpointed six metabolites with significant changes in aged ovaries compared to young controls. Phosphoethanolamine (PEA) showed the most pronounced decrease (Fig. 8) in aged ovaries

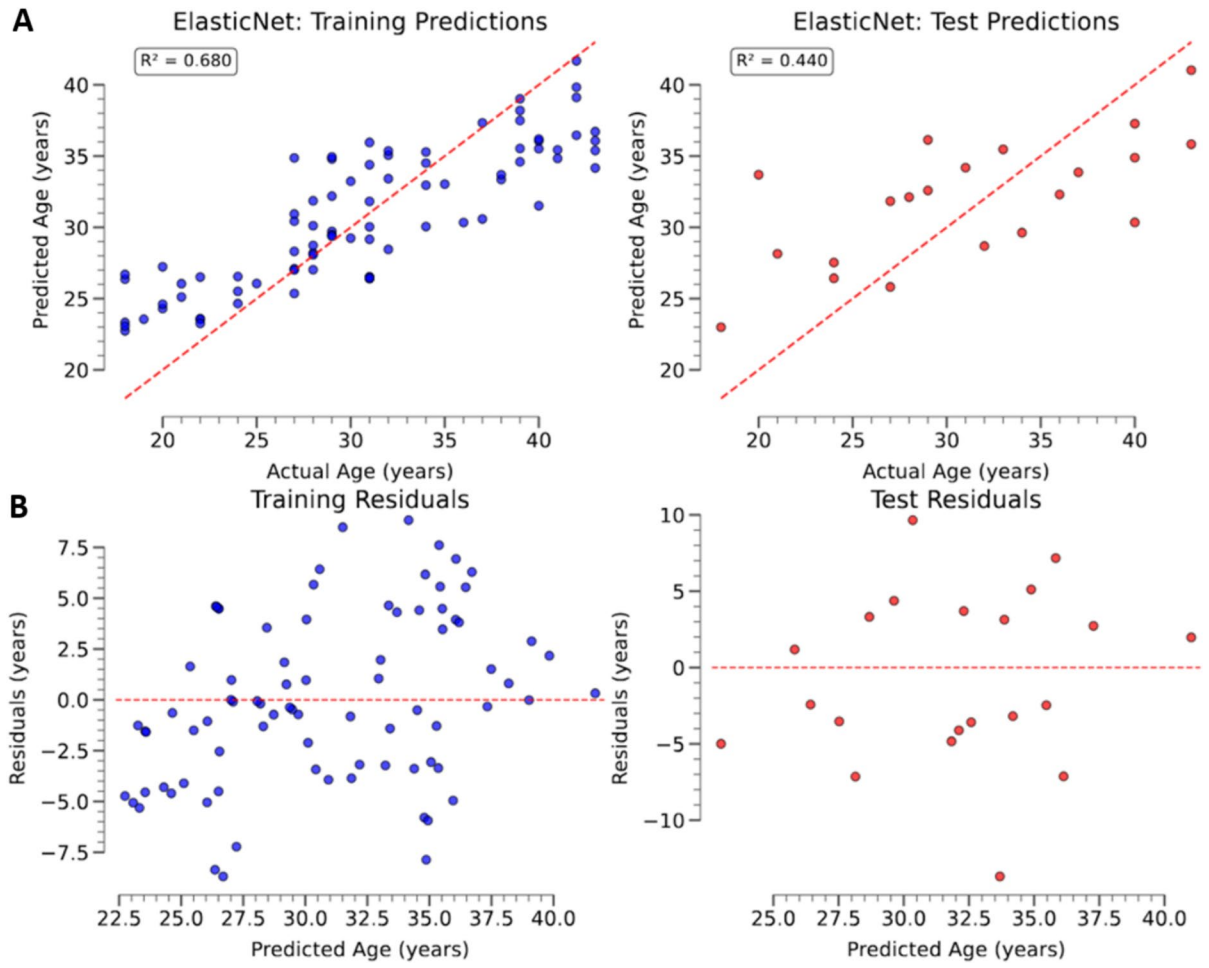

Fig. 6 Model prediction accuracy across age ranges. (**A**) Residual plot showing the distribution of prediction errors (predicted age—chronological age) across the age spectrum. The dashed line at y = 0 represents perfect prediction. Color gradient indicates age groups (e.g., 20–30, 30–35, 35–40, 40 + years), revealing whether prediction accuracy varies systematically with age. The left panel (Training set) displays a scatter plot of predicted age versus actual age, indicating a strong positive correlation. The dashed red line represents the ideal 1:1 relationship. The reported R^2 value of 0.680 indicates a good model fit and predictive performance on the training data. (**B**) Density plot comparing prediction errors across age groups, demonstrating the model's robustness for the training and test residuals. Left Panel: Residuals (prediction error in years) are plotted against predicted age. The residuals are centered around zero (dashed red line), with no strong systematic pattern, indicating reasonable model calibration on the training data. Right panel (Test residuals): The residuals for the test set show greater dispersion, including some larger positive and negative errors, which reflects increased variability and reduced precision when applied to unseen data

($p \leq 0.0001$). Moreover, the metabolites betaine, fructose-1,6-bisphosphate, pyruvate, and reduced glutathione (GSH) were significantly downregulated in the metabolome of the aged ovary. These age-associated metabolite changes suggest disruptions in key biochemical pathways, including lipid metabolism (PEA), glycolysis (fructose-1,6-bisphosphate and pyruvate), and redox homeostasis (GSH), as hallmarks of ovarian aging. In contrast, guanosine was significantly upregulated in aged ovaries compared to their younger counterparts (Fig. 8). A correlation heatmap (Fig. 9) further highlighted age-related patterns and interrelationships among the measured metabolites.

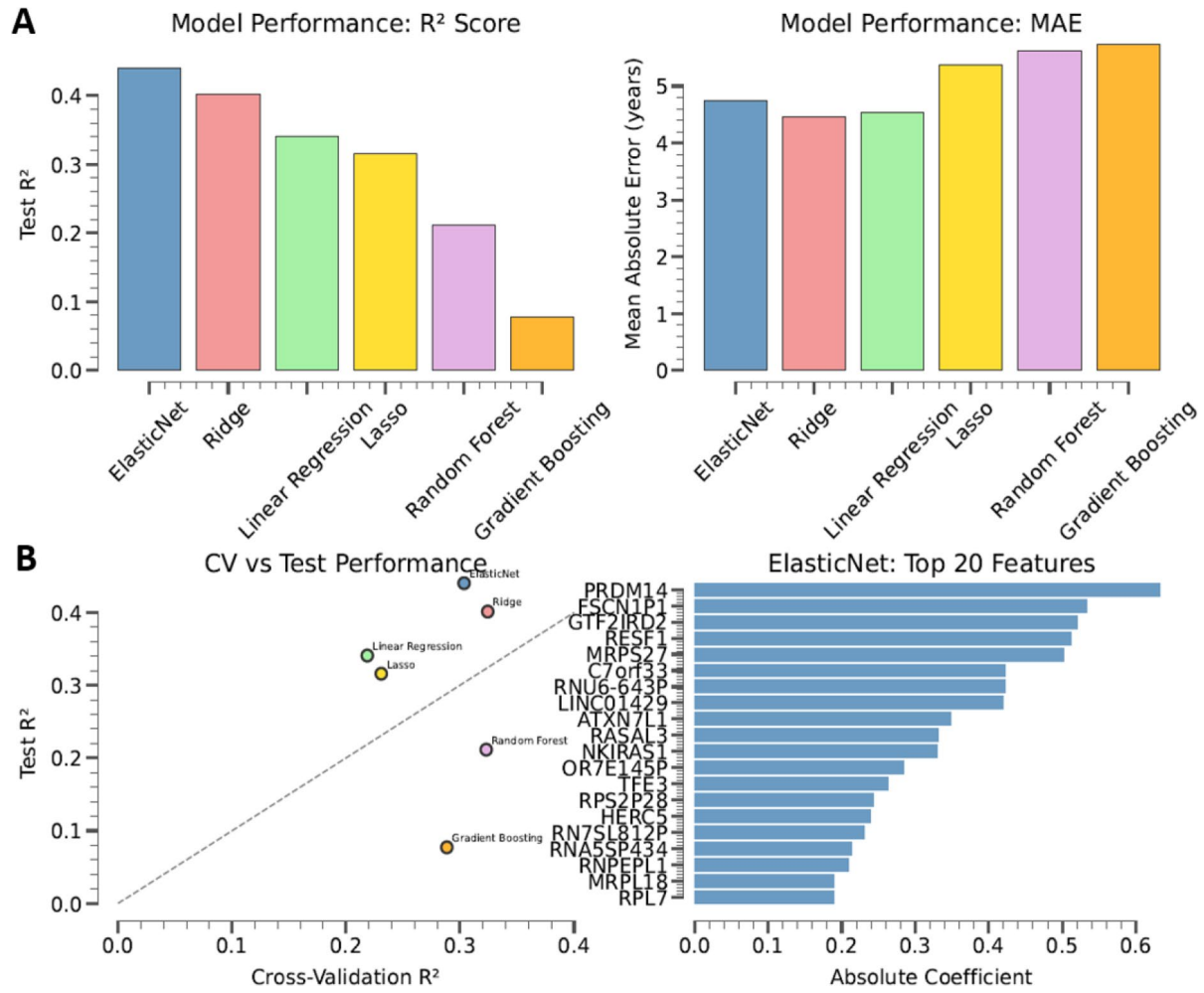

Fig. 7 Predictive performance of age-associated gene expression signatures. (**A**) Model performance comparison across Elastic Net, Ridge, linear regression, LASSO, random forest, and gradient boosting models, evaluated using test-set R^2 (left) and mean absolute error (MAE; right). (**B**) Cross-validation versus test-set R^2 for each model, illustrating generalization performance. Bar plot showing feature importance for the Elastic Net model, highlighting the top 20 genes ranked by absolute coefficient magnitude, which indicates the transcripts with the strongest contributions to biological age prediction in oocytes

Topological pathway enrichment of metabolites

The aim of enrichment analysis of metabolites is to reveal the biological pathways that play a critical role in a biological process, thereby providing a better understanding of the molecular mechanisms underlying these processes. Figure 10A illustrates the top 25 metabolic pathways, along with their respective enrichment rates and significance. The ubiquinone biosynthesis, glycerophospholipid metabolism, and sphingolipid metabolism pathways exhibit a significant ($p \leq 0.05$) enrichment ratio of greater than 2.5. This significant enrichment has also been confirmed by analysing the specific metabolite sets of the aforementioned pathways (Fig. 10B). With regard to the earlier-mentioned downregulation of PEA in aged ovaries, the top 25 metabolites that correlate with PEA are shown in Fig. 10C for a better understanding of the interaction with other metabolites. The sphingolipid metabolism, in which PEA plays a role, is depicted in Fig. 10D.

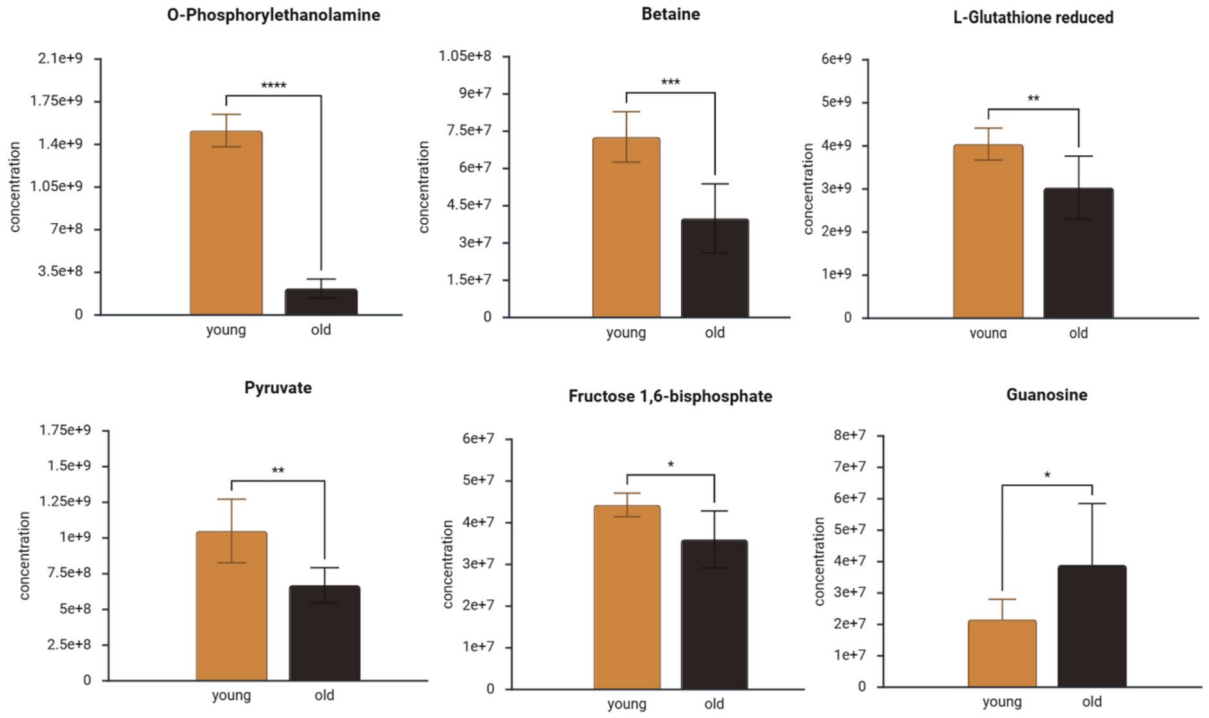

Fig. 8 Metabolite profiling in aged and young ovaries. Box plots showing the significantly upregulated metabolites and downregulated metabolites in the ovaries of both age groups. Asterisks indicate statistical significance: $*=p<0.05$, $**=p<0.01$, $***=p<0.001$, $****=p<0.0001$

Individual metabolic biomarkers for ovarian aging

To elucidate individual metabolic biomarkers for ovarian aging, we performed a classical univariate receiver operating characteristic (ROC) curve. Figure 11 shows the four top-ranked metabolites based on the area under the curve (AUC), suggesting that Phosphoethanolamine (AUC = 0.959) and Betaine (AUC = 0.959) are robust ($p<0.01$) candidates as metabolomic biomarkers for aging in murine ovaries. Moreover, pyruvate (AUC = 0.837) and reduced glutathione (AUC = 0.878) also appear to be reliable ($p<0.05$) candidates for metabolomic biomarkers of aging in murine ovaries, indicating their potential diagnostic value. This suggests that lower PEA, betainę, and pyruvate levels could be a marker for metabolic aging, not only systemically but also at the level of oocyte health. Since pyruvate is essential for maintaining mitochondrial function and protecting against oxidative stress, a decrease in pyruvate with age could signal increased oxidative damage, diminished mitochondrial function in oocytes, and accelerated ovarian aging. Therefore, this supports that pyruvate could serve as a predictive biomarker of ovarian aging.

Discussion

This study is the first to shed light on the metabolic changes between young and aged ovarian tissue samples, providing a better understanding of the underlying biological mechanisms of ovarian aging. Combining these results with RNA sequencing data has been used to identify biomarkers for combating reproductive aging in women. Therefore, the development of non-invasive and highly sensitive biomarkers capable of assessing oocyte and ovarian quality across a woman's reproductive lifespan is essential for future advancements in assisted reproductive technologies. Aging is a pervasive process characterized by the progressive decline of physiological functions and the increased susceptibility to chronic diseases. Specific

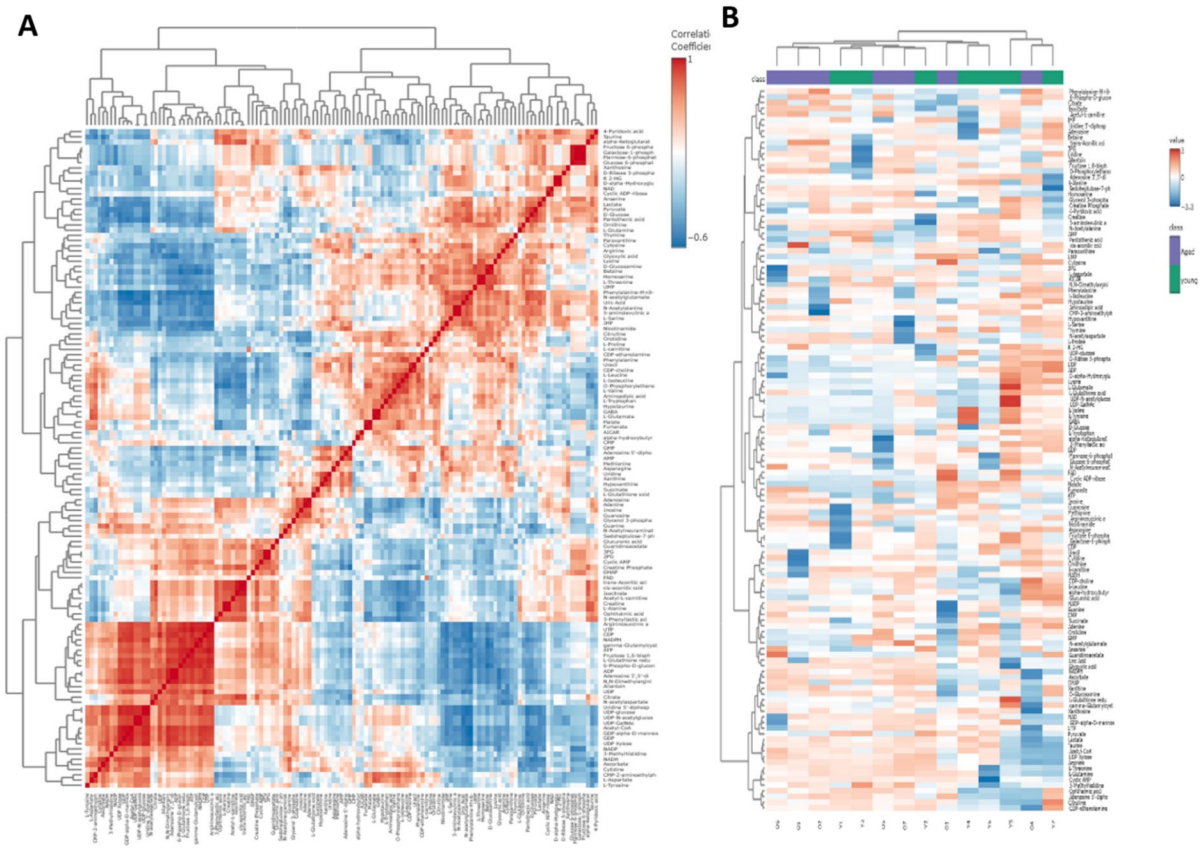

Fig. 9 Correlation heatmap of tested metabolites. (**A**) Each square represents the Spearman correlation coefficient between the metabolic phenotypes of the column and those of the row. The metabolic phenotype order is determined using hierarchical clustering with the 1-correlation distance function. The dissimilarity index is employed for cluster analysis to arrange different seed phenotypes according to their similarity. Self–self correlations are identified in dark red. (**B**) A heat map of differential metabolites visualized the variations in metabolite profiles between young and aged ovaries. The vertical axis represents the metabolites, and the horizontal axis indicates the sample class, comprising Y1-Y7 (ovaries from young donors) and O1-O7 (ovaries from old donors), as well as the grouping information. The cluster tree at the top of the figure is the similarity cluster of the distribution of metabolites in each sample, and the cluster tree at the left is the sample cluster tree. The relationship between color and Z-score is shown in the scale at the top right, ranging from 3 (red) to − 3.3 (blue)

hallmarks of aging help to understand this complex process [42, 43]. In women and other mammalian females, the aging process affects the reproductive system earlier and more profoundly than other organs, often preceding the onset of menopause. Reproductive aging also impacts overall health as ovarian hormones, particularly estrogen, regulate various organ systems downstream [44].

As we have presented, biological process terms related to mitochondrial function, such as electron transport and oxidative phosphorylation pathways, as well as processes related to stress responses, including apoptosis, immune response, and inflammation pathways, were significantly enriched terms for aged oocytes (Fig. 2). These findings indicate that oocyte aging is characterized by a coordinated decline in proteostasis, cellular organization, epigenetic regulation, and energy metabolism, concurrent with the activation of stress-response pathways. Moreover, the performed clustering analysis indicates a coordinated, age-dependent transcriptional reprogramming within the oocyte, characterized by the differential regulation of genes involved in diverse cellular pathways [36]. This bimodal expression pattern underscores the presence of multiple, interrelated biological processes that become progressively dysregulated during

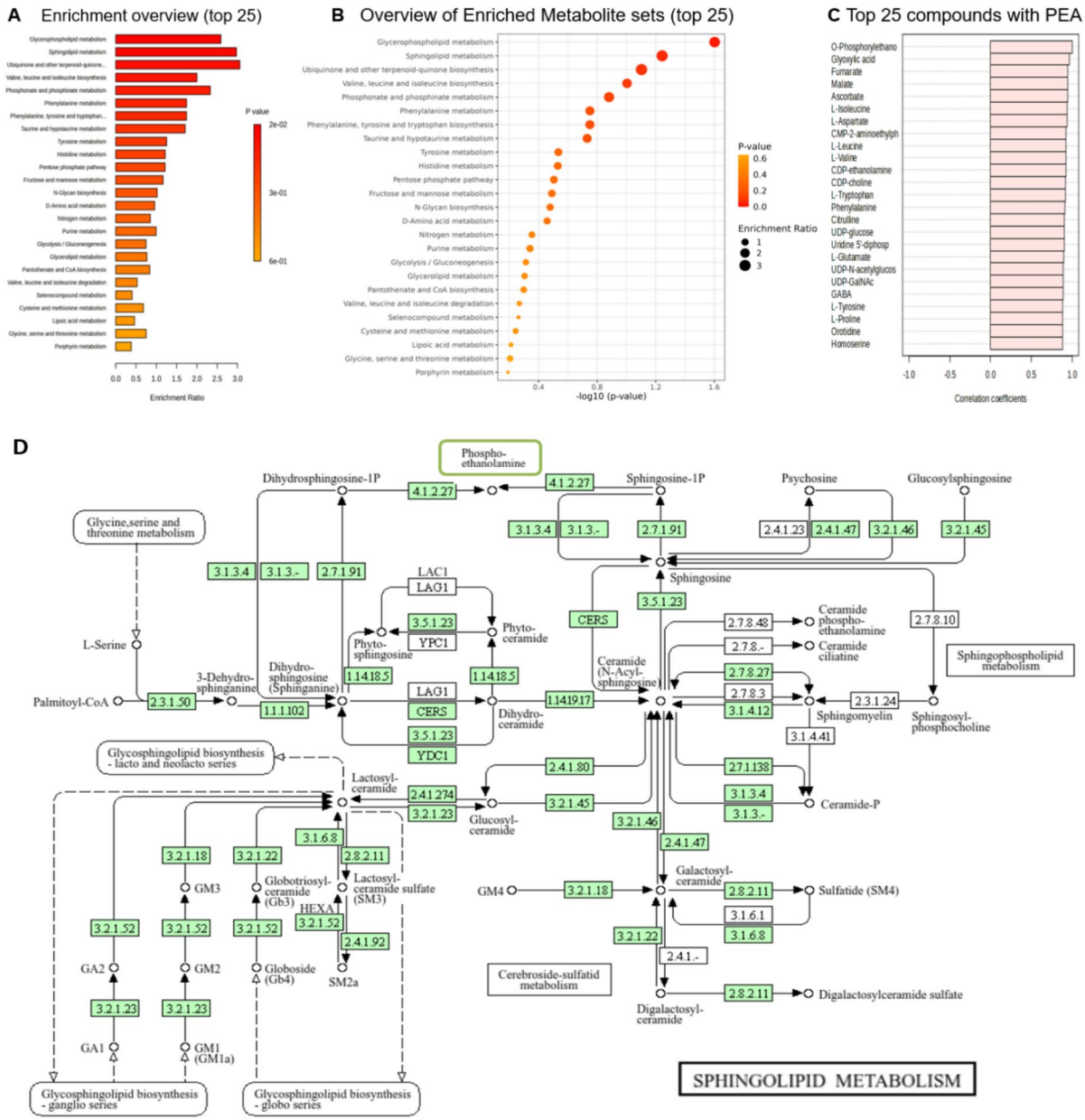

Fig. 10 Predictive Enrichment analysis of over-representation analysis and top enrichment analysis. (**A**) The abscissa represents the enrichment factor, which is the ratio of observed metabolites to theoretical metabolites in the metabolic pathway. The size of the *p*-value is expressed by color. The darker the color, the smaller the *p*-value. (**B**) Overview of top 25 enriched metabolite sets. (**C**) Top 25 compounds that correlate with PEA. (**D**) Scheme showing the sphingolipid metabolism. Sphingosine-1P (S1P) and Dihydrosphingosin-1P (DH-S1P) are involved in the biosynthesis of Phosphoethanolamine (box with the green outer line on the top). S1P and DH-S1P, generated from the phosphorylation of dihydrosphingosine, can be degraded to produce ethanolamine phosphate (Eth-P), which is utilized for phosphatidylethanolamine synthesis

oocyte aging, potentially contributing to the decline in oocyte quality observed with advancing maternal age [32–41]. Among the most predictive genes were *VCAM1*, *HERC5*, and *TNFRSF19*, which exhibited high importance scores. These genes have previously been implicated in cellular stress response, immune

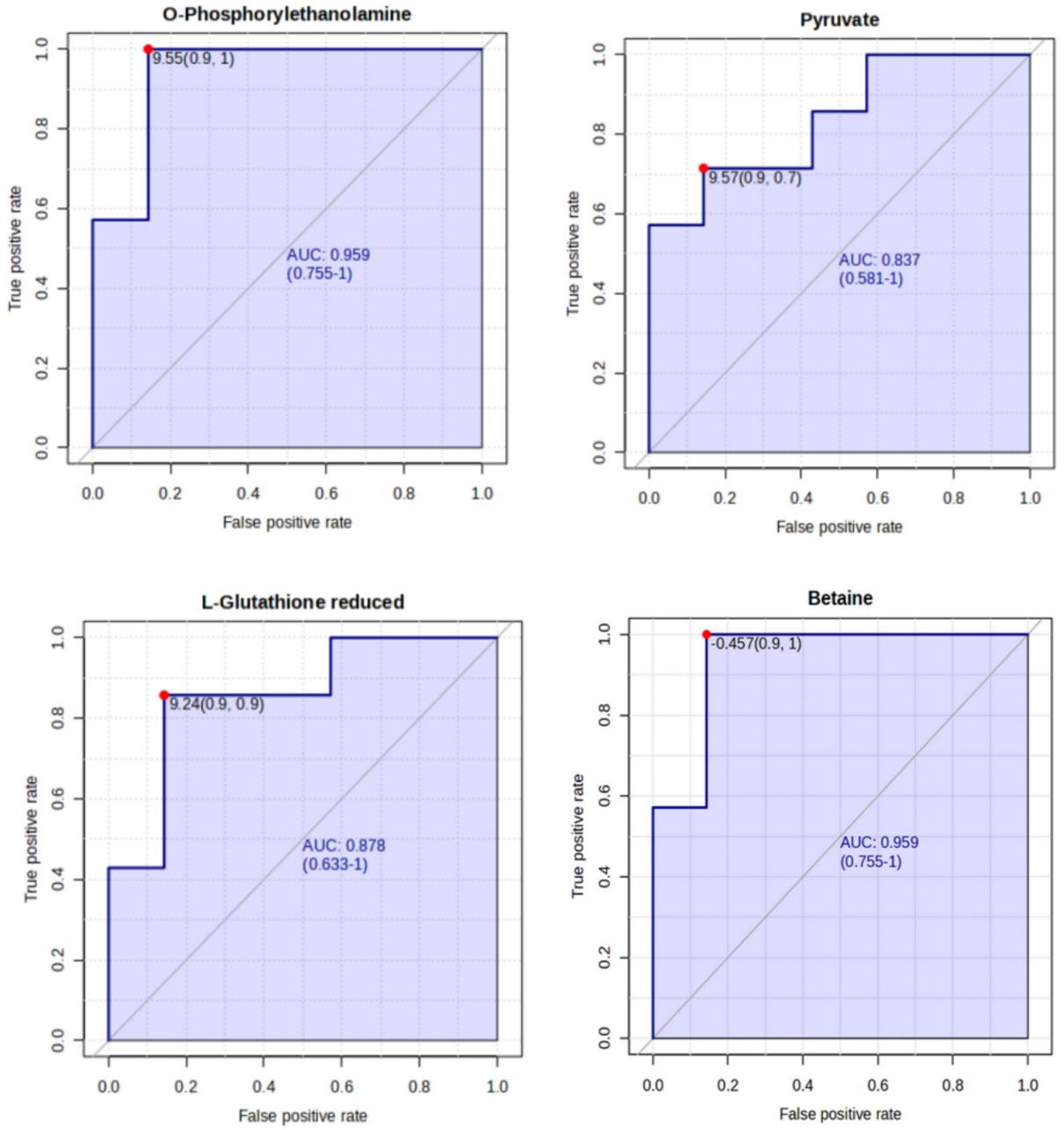

Fig. 11 Biomarker analysis. Top-ranked metabolites based on the area under the ROC curve (AUROC) identified by the non-targeted metabolomics analysis

signaling, and apoptotic regulation [45–59], supporting their biological relevance as potential biomarkers of oocyte aging. These findings demonstrate that age-associated gene expression signatures can reliably predict biological age in human oocytes, and that specific genes with high predictive importance may serve as mechanistic indicators of the molecular aging process in the female germline.

The integration of metabolite-based biomarkers into clinical practice facilitates more accurate diagnoses, personalized treatment plans, and, ultimately, improved reproductive outcomes. It is worth

mentioning that the lipid metabolism is central to ovarian physiology and oocyte function, as it drives energy production through β-oxidation of fatty acids, which is essential for maturation and embryogenesis [60, 61]. However, as women age, lipid metabolism efficiency decreases, leading to impaired oocyte maturation and a decline in fertility [62, 63]. As we have shown in our metabolite profiling, PEA was significantly downregulated in aged ovaries (Fig. 8), and this metabolite appears to be a potential biomarker for reproductive aging in females (Fig. 11). To the best of our knowledge, we are the first group showing that PEA also plays a role in ovarian aging. However, the role of PEA in the ovarian aging process remains elusive.

Previous research has provided evidence that PEA is the ethanolamine monoester of phosphoric acid and a metabolite of phospholipid metabolism [64]. This phosphomonoester shows strong structural similarity to the inhibitory neurotransmitter gamma-aminobutyric acid (GABA) [64]. Alpha-glyceryl-PEA has been reported to slow down aging of human neural stem cells [65]. This could also be an interesting feature relevant to the ovary, suggesting that low levels of PEA could accelerate the ovarian aging process. Furthermore, PEA is involved in modulating the fluidity and flexibility of membranes, thus supporting membrane protein functions necessary for effective cellular signalling and transport [66, 67].

Interestingly, it has been demonstrated that fibrosis and the stiffness of ovarian tissue are aging-related phenotypes that diminish the physiological function of the ovary [68]. Given the importance of cell membrane composition in the context of cellular aging further research into the regulatory roles of PEA and its interaction with other phospholipids remains imperative. As shown in Fig. 10, PEA is also involved in sphingolipid metabolism, and our results demonstrate enrichment in this pathway (Fig. 10). Changes in sphingolipid metabolites are associated with aging and prevalent conditions like diabetes and cancer, as well as neurodegenerative, cardiovascular, and respiratory disorders [69–72]. It is now well-documented that sphingolipids regulate a host of signals within the cell, controlling a myriad of functions, including cell growth and differentiation, inflammation, immune functions, and the differentiation of the nervous system [73, 74]. Sphingolipids contribute to apoptosis by either clustering lipid microdomains or acting as second messengers, binding specific proteins and modulating their phosphorylation [75, 76]. In apoptosis, sphingolipids can influence mitochondria through various mechanisms, including the formation of ceramide channels, which may contribute to mitochondrial outer membrane permeability (MOMP), the activation of kinases, and the inhibition of respiration [77, 78].

The latter findings align with our results from the Gene Ontology enrichment analysis, which revealed alterations in key biological processes, including those related to mitochondrial function and stress responses, such as apoptosis, immune response, and inflammatory pathways, that are affected by oocyte aging (Fig. 2). In the context of these results, it is worth noting that mitochondrial dysfunction is a hallmark of aging in the ovary and oocytes, resulting in decreased energy production, which is essential for cellular processes such as chromosomal alignment and segregation during meiosis [79]. Mitochondrial membrane potential, which reflects the functional status of the electron transport chain, is another critical marker, as its decline reflects impaired cellular respiration and increased susceptibility to apoptosis [80, 81]. Mitochondria of senescent cells often reduce ATP production and elevate reactive oxygen species (ROS) [82]. Consequently, energy metabolism is redirected towards glycolysis. To regenerate NAD + levels for glycolytic flow and sustain redox balance, lactate dehydrogenase (LDH) converts cytosolic pyruvate into lactate [83, 84]. Mitochondrial pyruvate transport is crucial for proper embryonic development [85] and for the physiological function of the ovary throughout a woman's life [86]. As shown in our results (Fig. 8), pyruvate was significantly downregulated in the aged ovaries and could, therefore, also serve as a metabolomic-based biomarker (Fig. 11). Pyruvate plays a critical role in oocyte metabolism and maturation, directly influencing both physiological and aging-related processes. The consumption and utilization of pyruvate during oocyte development have been well-established as essential for maintaining energy homeostasis, cellular integrity, and proper metabolic function [87].

Throughout oocyte development, pyruvate is utilized alongside oxygen, and its consumption increases significantly as the oocyte progresses from primary to pre-ovulatory stages within the ovarian follicle [88]. This suggests that pyruvate is a critical

energy substrate, particularly in mitochondrial function during oocyte maturation [88]. Oocytes that rely on pyruvate show increased energy needs. In addition, studies reveal that pyruvate's role is not limited to energy production. It is also involved in reducing oxidative stress and supporting mitochondrial electron transport, a process necessary for ooplasmic maturation. In experiments where pyruvate was used as the primary energy source, oocytes demonstrated better maturation and reduced oxidative damage, especially when glucose metabolism was inhibited [89]. This highlights pyruvate's dual role: supporting bioenergetics while safeguarding cellular components against oxidative aging. Pyruvate's antioxidant properties may slow this process by mitigating the accumulation of reactive oxygen species (ROS). This is especially important given that elevated ROS levels are associated with cellular aging and decreased oocyte quality [89]. Pyruvate consumption is tightly linked to both the energy production needs and antioxidative defense mechanisms within the ovary and oocytes. Therefore, fluctuations in pyruvate levels could signal the onset of mitochondrial dysfunction or an increase in oxidative stress, both of which are indicative of oocyte aging. Hence, monitoring serum pyruvate levels might provide a non-invasive marker for assessing oocyte health and predicting oocyte aging-related fertility issues. Another metabolite, which was significantly downregulated in aged ovaries, is Betaine (Fig. 8). Betaine is an osmolyte and methyl donor, plays a multifaceted role in the aging process through various mechanisms, including its involvement in one-carbon metabolism, reduction of homocysteine levels, antioxidant and anti-inflammatory activities, and influence on mitochondrial function and cellular senescence [90–94]. Betaine acts as a crucial methyl donor in one-carbon metabolism, helping to maintain cellular S-adenosylmethionine levels, which are vital for numerous biological reactions, including DNA methylation. By reducing concentrations of homocysteine, a known risk factor for cardiovascular and neurodegenerative diseases, betaine helps to mitigate vascular, neurodegenerative, and oxidative damage associated with aging [90, 91]. Moreover, Betaine demonstrates significant antioxidant and anti-inflammatory activities, which are critical in combating the chronic low-grade inflammation, also known as "inflammaging" and oxidative stress that characterize aging [90, 91]. Previous research has provided evidence that betaine intervention can delay age-related muscle loss by improving muscle mass, strength, and function, partly by mitigating the impairment in mitochondrial respiration induced by Mss51 [92]. Recent integrated multi-omics analyses suggest that betaine metabolism is enhanced by exercise and that betaine itself may act as an "exercise mimetic." Exercise-driven betaine enrichment can exert geroprotective effects, helping to rescue age-related health decline in mice, partly by reducing cellular senescence and inflammation [93]. This positions betaine as a promising candidate for promoting healthy aging [94]. Betaine supplementation has been shown to improve sperm motility in mouse models with genetic defects in choline dehydrogenase, a pathway essential for betaine synthesis, which is linked to idiopathic male factor infertility in humans [95]. Beyond male fertility, betaine has demonstrated an ability to improve the development of ethanol-treated mouse embryos, suggesting a role in mitigating the adverse effects of ethanol exposure on embryo development in women undergoing assisted reproductive technologies [96]. It can also enhance nucleic acid methylation important for oocyte meiotic maturation when supplemented in IVF media [97]. Animal studies also highlight betaine's capacity to improve semen quality, antioxidant status, and DNA repair under stress conditions like heat [98]. Furthermore, high concentrations of betaine have shown detrimental effects on sperm motility in some cryopreservation contexts [99]. The direct therapeutic application of modulating PEA levels for infertility treatment is not yet clearly established from current research [100]. The presented changes in PEA levels might represent consequences of ovarian aging rather than primary targets for intervention. The complex nature of PEA metabolism requires a deeper understanding of how to effectively and safely manipulate PEA pathways for fertility benefits.

Conclusions

In conclusion, this study provides a comprehensive multi-level characterization of the molecular and metabolic hallmarks underlying oocyte and ovarian aging. Our data confirm that advanced maternal age

profoundly impairs reproductive potential, as reflected by reduced implantation and ongoing pregnancy rates, as well as distinct morphological alterations in oocytes from women over 35 years of age. The concomitant decline in AMH levels and elevation in FSH concentrations further reinforce the established endocrine signatures of diminished ovarian reserve and reproductive competence. At the transcriptomic level, integrative gene expression analyses revealed coordinated dysregulation of multiple biological pathways central to oocyte functionality. Enrichment of mitochondrial, apoptotic, and immune-related processes highlights the multifactorial nature of age-related oocyte deterioration. Hierarchical clustering and machine learning analyses consistently identified *VCAM1*, *HERC5*, and *TNFRSF19* as among the most predictive biomarkers of maternal age, emphasizing their mechanistic and diagnostic relevance. The ability of gene expression signatures to accurately predict biological age underscores their potential as molecular indicators for assessing oocyte quality and reproductive lifespan. Complementary metabolomic profiling of ovarian tissues revealed profound metabolic remodeling with age, notably involving phosphoethanolamine, betaine, pyruvate, and reduced glutathione. Both phosphoethanolamine and betaine show emerging clinical relevance for infertility, primarily as biomarkers and potential therapeutic supplements, respectively. Their roles stem from their fundamental functions in cellular metabolism, membrane integrity, and epigenetic regulation. Our multi-omic findings provide a comprehensive framework that links molecular, metabolic, and functional alterations during reproductive aging. They holistic view on candidate biomarkers and mechanistic pathways that may serve as targets for therapeutic or diagnostic strategies aimed at mitigating the decline in female reproductive health with advancing age.

Outlook

The future of managing oocyte and ovarian aging is poised for a significant transformation, driven by the increasing emphasis on personalized therapeutic strategies through the integration of multi-omics. This approach, which encompasses technologies such as transcriptomics and metabolomics, is fundamental to the advancement of precision medicine in reproductive health. It promises to move beyond conventional standardized interventions, allowing for the tailoring of treatments to comprehensive biological profiles that reflect each patient's unique pathophysiology.

By analyzing individual metabolomic profiles, clinicians will be empowered to design precision therapies that meticulously address both endocrine disruptions and metabolic dysfunctions contributing to ovarian senescence. This represents a significant step towards optimizing reproductive outcomes for women facing the challenges of reproductive aging. The most immediate clinical translation for PEA lies in its potential as a diagnostic tool. Profiling PEA and its related lipids in follicular fluid or seminal plasma could help identify specific metabolic dysfunctions contributing to infertility, guiding more personalized treatment approaches. Detailed mechanistic research is required to elucidate how specific PEA dysregulations directly impair reproductive function. This would involve studying the effects of exogenous PEA or specific enzyme modulators on gamete quality, fertilization, and embryo development. Moreover, large-scale prospective studies are needed to validate PEA as a robust diagnostic biomarker across diverse infertility etiologies. Intervention studies, once preclinical mechanisms are clearer, would be crucial to assess whether targeted modulation of PEA metabolism can improve fertility outcomes in humans. Betaine's role in counteracting elevated homocysteine, improving sperm quality, and potentially protecting embryos suggests it could be a valuable, relatively low-risk dietary supplement, particularly for men with specific sperm motility issues. Further research is needed to elucidate the precise mechanisms by which betaine affects gamete quality and embryo development in various animal models of infertility, thereby establishing optimal concentrations and durations of supplementation. The development of non-invasive and highly sensitive biomarkers capable of assessing oocyte quality across a woman's reproductive lifespan is essential for future advancements. Artificial intelligence and machine learning could play a transformative role by enabling the creation of predictive models that combine physiological, molecular, and genetic markers for oocyte and ovarian aging.

Acknowledgements We would like to thank all patients who participated in this study. During the preparation of this manuscript, the authors utilized Grammarly to enhance the accuracy of the English language and improve the reading flow. The authors have reviewed and edited the output and take full responsibility for the content of this publication.

Author contribution P.K.: Participation in study design, execution, analysis, manuscript writing, and critical discussion; A.K.Y.: Participation in analysis and manuscript reviewing; S.J. and X.G.: Participation in analysis and manuscript reviewing; J.K. and J.W.: Participation in patient data collection and analysis; M.C.H.: Scientific supervision and support.

Funding P.K. received the IDUB Mobility Grant from Nicolaus Copernicus University (Grant Nr 75/2022). This research was funded by the National Science Centre, grant number OPUS28/2024/55/B/NZ9/02063.

Data Availability Data will be made available on request.

Declarations

Ethics approval Institutional ethics committee approval (KBKA/07/O/2024, annex KBKA/06/2025) was obtained.

Consent to participate Informed consent was obtained from all patients involved in the study.

Conflict of interest Marcia C. Haigis reports personal/consulting fees from Alixia and Mitoq outside the submitted work. The other authors declare no Competing Financial or Non-Financial Interests.

References

1. Walter KL. Ovarian aging and fertility. JAMA. 2025. https://doi.org/10.1001/jama.2025.2361.
2. Santoro N, Polotsky AJ. Infertility evaluation and treatment. N Engl J Med. 2025;392(11):1111–9. https://doi.org/10.1056/NEJMcp2311150.
3. Adam D. How far will global population rise? Researchers can't agree. Nature. 2021;597(7877):462–5. https://doi.org/10.1038/d41586-021-02522-6.
4. Aitken RJ. The changing tide of human fertility. Hum Reprod. 2022;37(4):629–38. https://doi.org/10.1093/humrep/deac011.
5. Lutz W, Sanderson W, Scherbov S. The coming acceleration of global population ageing. Nature. 2008;451(7179):716–9. https://doi.org/10.1038/nature06516.
6. Mastenbroek S, de Wert G, Adashi EY. The imperative of responsible innovation in reproductive medicine. N Engl J Med. 2021;385:2096–100. https://doi.org/10.1056/NEJMsb2101718.
7. Bertoldo MJ, Listijono DR, Ho WJ, Riepsamen AH, Goss DM, Richani D, et al. NAD+ repletion rescues female fertility during reproductive aging. Cell Rep. 2020;30(6):1670-1681.e7. https://doi.org/10.1016/j.celrep.2020.01.058.
8. Sgueglia G, Longobardi S, Valerio D, Campitiello MR, Colacurci N, Di Pietro C, et al. The impact of epigenetic landscape on ovarian cells in infertile older women undergoing IVF procedures. Clin Epigenetics. 2023;15:76. https://doi.org/10.1186/s13148-023-01490-0.
9. Muka T, Oliver-Williams C, Kunutsor S, Laven JS, Fauser BC, Chowdhury R, et al. Association of age at onset of menopause and time since onset of menopause with cardiovascular outcomes, intermediate vascular traits, and all-cause mortality: a systematic review and meta-analysis. JAMA Cardiol. 2016;1(7):767–76. https://doi.org/10.1001/jamacardio.2016.2415.
10. Collaborative Group on Hormonal Factors in Breast Cancer. Menarche, menopause, and breast cancer risk: individual participant meta-analysis, including 118 964 women with breast cancer from 117 epidemiological studies. Lancet Oncol. 2012; 13(11):1141–1151.https://doi.org/10.1016/S1470-2045(12)70425-4
11. Cargill SL, Carey JR, Müller HG, Anderson G. Age of ovary determines remaining life expectancy in old ovariectomized mice. Aging Cell. 2003;2(3):185–90. https://doi.org/10.1046/j.1474-9728.2003.00049.x.
12. Chen F, Spiessens C, D'Hooghe T, Peeraer K, Carpentier S. Follicular fluid biomarkers for human in vitro fertilization outcome: proof of principle. Proteome Sci. 2016;14:17. https://doi.org/10.1186/s12953-016-0106-9.
13. Albeitawi S, Bani-Mousa SU, Jarrar B, Aloqaily I, Al-Shlool N, Alsheyab G, et al. Associations between follicular fluid biomarkers and IVF/ICSI outcomes in normo-ovulatory women-a systematic review. Biomolecules. 2025;15(3):443. https://doi.org/10.3390/biom15030443.
14. Zhou M, Qin Z, Zhu X, Ruan Y, Ling H, Li C, et al. Pyruvate dehydrogenase kinases: key regulators of cellular metabolism and therapeutic targets for metabolic diseases. J Physiol Biochem. 2025;81(1):21–34. https://doi.org/10.1007/s13105-025-01068-9.
15. Hayat N, Akram Z, Khalid N, Ullah NR, Mazhar T. Link between iron-mediated lipid peroxidation and polycystic ovary syndrome (PCOS): exploring the genes underlying iron regulatory mechanism. J Ovarian Res. 2025;18(1):48. https://doi.org/10.1186/s13048-024-01562-6.
16. Kolesnikova LI, Krusko OV, Belenkaya LV, Sholokhov LF, Grebenkina LA, Kurashova NA, et al. Changes in the lipid peroxidation-antioxidant protection system in women with ovarian hyperandrogenism at different periods of reproductive age. Bull Exp Biol Med. 2021;170(3):308–11. https://doi.org/10.1007/s10517-021-05057-y.
17. Huang R, Xue X, Li S, Wang Y, Sun Y, Liu W, et al. Alterations of polyunsaturated fatty acid metabolism in ovarian tissues of polycystic ovary syndrome rats. J Cell Mol Med. 2018;22(7):3388–96. https://doi.org/10.1111/jcmm.13614.
18. Zhou J, Zuo W, Tan Y, Wang X, Zhu M, Zhang H. Effects of n-3 polyunsaturated fatty acid on metabolic status in women with polycystic ovary syndrome: a meta-analysis of randomized controlled trials. J Ovarian Res. 2023;16(1):54. https://doi.org/10.1186/s13048-023-01130-4.
19. Zarezadeh R, Nouri M, Hamdi K, Shaaker M, Mehdizadeh A, Darabi M. Fatty acids of follicular fluid

phospholipids and triglycerides display distinct association with IVF outcomes. Reprod Biomed Online. 2021;42(2):301–9. https://doi.org/10.1016/j.rbmo.2020.09.024.
20. Chen Y, Touboul R, Chen Y, Chang CL. Strategic delivery of omega-3 fatty acids for modulating inflammatory neurodegenerative diseases. Front Aging Neurosci. 2025;17:1535094. https://doi.org/10.3389/fnagi.2025.1535094.
21. Giblin A, Cammack AJ, Blomberg N, Anoar S, Mikheenko A, Carcolé M, et al. Neuronal polyunsaturated fatty acids are protective in ALS/FTD. Nat Neurosci. 2025. https://doi.org/10.1038/s41593-025-01889-3.
22. Panda P, Ferreira CR, Cooper BR, Schaser AJ, Aryal UK. Multiplatform lipid analysis of the brain of aging mice by mass spectrometry. J Proteome Res. 2025;24(3):1077–91. https://doi.org/10.1021/acs.jproteome.4c00688.
23. Tighanimine K, Nabuco Leva Ferreira Freitas JA, Nemazanyy I, Bankolé A, Benarroch-Popivker D, et al. A homeostatic switch causing glycerol-3-phosphate and phosphoethanolamine accumulation triggers senescence by rewiring lipid metabolism. Nat Metab. 2024;6(2):323–42. https://doi.org/10.1038/s42255-023-00972-y.
24. Xu H, Li W, Huang L, He X, Xu B, He X, et al. Phosphoethanolamine cytidylyltransferase ameliorates mitochondrial function and apoptosis in hepatocytes in T2DM in vitro. J Lipid Res. 2023;64(3):100337. https://doi.org/10.1016/j.jlr.2023.100337.
25. Grapentine S, Agarwal P, Dolinsky VW, Bakovic M. Epigenome-wide methylation analysis shows phosphonoethylamine alleviates aberrant DNA methylation in NASH caused by Pcyt2 deficiency. PLoS ONE. 2025;20(3):e0320510. https://doi.org/10.1371/journal.pone.0320510.
26. Wyroba J, Kochan J, Kelley L, Iqbal S, Kordowitzki P. Anti-Müllerian hormone concentrations in women of different reproductive age and the chances of IVF outcome: a paradigm shift is needed. Aging Dis. 2025. https://doi.org/10.14336/AD.2024.1615.
27. Ozcan P, Sezer F, Altun A, Yildiz C, Timur HT, Keles EC, et al. Potential ability of circulating INSL3 level for the prediction of ovarian reserve and IVF success as a novel theca cell-specific biomarker in women with unexplained infertility and diminished ovarian reserve. Reprod Biol Endocrinol. 2025;23(1):40. https://doi.org/10.1186/s12958-025-01367-2.
28. Cakiroglu Y, Yuceturk A, Karaosmanoglu O, Kopuk SY, Korun ZEU, Herlihy N, et al. Ovarian reserve parameters and IVF outcomes in 510 women with poor ovarian response (POR) treated with intraovarian injection of autologous platelet rich plasma (PRP). Aging (Albany NY). 2022;14(6):2513–23. https://doi.org/10.18632/aging.203972.
29. Chong J, Xia J. Metaboanalystr: an R package for flexible and reproducible analysis of metabolomics data. Bioinformatics. 2018;34(24):4313–4. https://doi.org/10.1093/bioinformatics/bty528.
30. Westerhuis JA, van Velzen EJ, Hoefsloot HC, Smilde AK. Multivariate paired data analysis: multilevel PLS-DA versus OPLS-DA. Metabolomics. 2010;6(1):119–28. https://doi.org/10.1007/s11306-009-0185-z.
31. Nordström A, O'Maille G, Qin C, Siuzdak G. Nonlinear data alignment for UPLC-MS and HPLC-MS based metabolomics: quantitative analysis of endogenous and exogenous metabolites in human serum. Anal Chem. 2006;78(10):3289–95. https://doi.org/10.1021/ac060245f.
32. Reyes JM, Silva E, Chitwood JL, Schoolcraft WB, Krisher RL, Ross PJ. Differing molecular response of young and advanced maternal age human oocytes to IVM. Hum Reprod. 2017;32:2199–208.
33. Ferrero H, Corachán A, Aguilar A, Quiñonero A, Carbajo-García MC, Alamá P, et al. Single-cell RNA sequencing of oocytes from ovarian endometriosis patients reveals a differential transcriptomic profile associated with lower quality. Hum Reprod. 2019;34:1302–12.
34. Li J, Lu M, Zhang P, Hou E, Li T, Liu X, et al. Aberrant spliceosome expression and altered alternative splicing events correlate with maturation deficiency in human oocytes. Cell Cycle. 2020;19:2182–94.
35. Yu B, Doni Jayavelu N, Battle SL, Mar JC, Schimmel T, Cohen J, et al. Single-cell analysis of transcriptome and DNA methylome in human oocyte maturation. PLoS ONE. 2020;15:e0241698.
36. Zhang X, Yang J, Yang W, Cui N, Duan T, Li S, et al. Discordant effects of maternal age on the human MII oocyte transcriptome. Mol Hum Reprod. 2025;31(3):gaaf038. https://doi.org/10.1093/molehr/gaaf038.
37. Lee AWT, Ng JKW, Liao J, Luk AC, Suen AHC, Chan TTH, et al. Single-cell RNA sequencing identifies molecular targets associated with poor in vitro maturation performance of oocytes collected from ovarian stimulation. Hum Reprod. 2021;36:1907–21.
38. Llonch S, Barragán M, Nieto P, Mallol A, Elosua-Bayes M, et al. Single human oocyte transcriptome analysis reveals distinct maturation stage-dependent pathways impacted by age. Aging Cell. 2021;20:e13360.
39. Takeuchi H, Yamamoto M, Fukui M, Inoue A, Maezawa T, Nishioka M, et al. Single-cell profiling of transcriptomic changes during in vitro maturation of human oocytes. Reprod Med Biol. 2022;21:e12464.
40. Gonzalez XV, Almutlaq A, Gupta SS. Systematic review of mRNA expression in human oocytes: understanding the molecular mechanisms underlying oocyte competence. J Assist Reprod Genet. 2023;40:2283–95.
41. Darde TA, Lecluze E, Lardenois A, Stéevant I, Alary N, Tüttelmann F, et al. The ReproGenomics Viewer: a multi-omics and cross-species resource compatible with single-cell studies for the reproductive science community. Bioinformatics. 2019;35:3133–9.
42. López-Otín C, Blasco MA, Partridge L, Serrano M, Kroemer G. Hallmarks of aging: an expanding universe. Cell. 2023;186(2):243–78. https://doi.org/10.1016/j.cell.2022.11.001.
43. Balough JL, Dipali SS, Velez K, Kumar TR, Duncan FE. Hallmarks of female reproductive aging in physiologic aging mice. Nat Aging. 2024;4(12):1711–30. https://doi.org/10.1038/s43587-024-00769-y.
44. Jin C, Wang X, Yang J, Kim S, Hudgins AD, et al. Molecular and genetic insights into human ovarian

aging from single-nuclei multi-omics analyses. Nat Aging. 2025;5(2):275–90. https://doi.org/10.1038/s43587-024-00762-5.
45. Wang T, Tian J, Jin Y. VCAM1 expression in the myocardium is associated with the risk of heart failure and immune cell infiltration in myocardium. Front Cardiovasc Med. 2024;8:753177.
46. Singh V, Kaur R, Kumari P, Singh R. ICAM-1 and VCAM-1: gatekeepers in various inflammatory and cardiovascular disorders. Arch Med Sci. 2023;19:1163–72.
47. Zhang H, Shang J, Li W, Chen J. Increased expression of VCAM1 on brain endothelial cells drives blood–brain barrier impairment following chronic cerebral hypoperfusion. Aging Dis. 2024;15:167.
48. Ley K, Huo Y. VCAM-1 is critical in atherosclerosis. J Clin Invest. 2001;107:1213–5.
49. Marui N, Offermann MK, Swerlick RA, Kunsch C, Ahmad NM. Vascular cell adhesion molecule-1 gene transcription and expression are regulated through an antioxidant-sensitive mechanism in human vascular endothelial cells. J Clin Invest. 1993;92:1866–74.
50. Wong JJY, Pung YF, Sze SK, Liew LK. HERC5 is an IFN-induced HECT-type E3 protein ligase that mediates type I IFN-induced ISGylation of protein targets. Proc Natl Acad Sci USA. 2006;103:10735–40.
51. Dastur A, Beaudenon S, Kelley ML, Huibregtse JM. Herc5, an interferon-induced HECT E3 enzyme, is required for conjugation of ISG15 in human cells. J Biol Chem. 2005;280:19688–94.
52. Mathieu NA, Paparisto E, Barr SD, Huibregtse JM. HERC5 and the ISGylation pathway: critical modulators of the antiviral immune response. Viruses. 2021;13:2276.
53. Jacquet S, Pontier D, Etienne L. Rapid evolution of HERC6 and duplication of a chimeric HERC5/6 gene in rodents and bats suggest an overlooked role of HERCs in mammalian immunity. Front Immunol. 2020;11:574046.
54. Schneegans S, Löptien J, Mojzisch A, Fuhrmann B, Glüer S, et al. HERC5 downregulation in non-small cell lung cancer is associated with altered energy metabolism and metastasis. Cancer Metab. 2024;12:2.
55. Shao L, Zuo X, Yang Y, Zhang X, Song W. The inherited variations of a p53-responsive enhancer in 13q12.12 confer lung cancer risk by attenuating TNFRSF19 expression. Cell Death Differ. 2019;26:163–75.
56. Hu S, Tamada K, Ni J, Wang S. Characterization of TNFRSF19, a novel member of the tumor necrosis factor receptor superfamily. Biochem Biophys Res Commun. 1999;266:166–71.
57. Guo P, Huang J, Zhang J, Ma L. The potential role of circRNA_004229 in hair/epidermal regulation after MED1 ablation in keratinocytes. RSC Adv. 2019;9:22533–40.
58. Devarapu SK, Grill JF, Junhui X, Müller B. Tumor necrosis factor superfamily ligand mRNA expression profiles differ between humans and mice during homeostasis and between various murine kidney injuries. J Biomed Sci. 2017;24:77.
59. Dong Y, Zhou H, Alhaskawi A, Zhang Y. Alterations in bone fracture healing associated with TNFRSF signaling pathways. Front Endocrinol. 2022;13:938647.
60. Jensen JT, Addis IB, Hennebold JD, Bogan RL. Ovarian lipid metabolism modulates circulating lipids in premenopausal women. J Clin Endocrinol Metab. 2017;102(9):3138–45. https://doi.org/10.1210/jc.2016-3456.
61. Zhang L, Zhao J, Lam SM, Chen L, Gao Y, Wang W, et al. Low-input lipidomics reveals lipid metabolism remodelling during early mammalian embryo development. Nat Cell Biol. 2024;26(2):278–93. https://doi.org/10.1038/s41556-023-01341-3.
62. Ko SH, Jung Y. Energy metabolism changes and dysregulated lipid metabolism in postmenopausal women. Nutrients. 2021;13(12):4556. https://doi.org/10.3390/nu13124556.
63. Mutlu AS, Duffy J, Wang MC. Lipid metabolism and lipid signals in aging and longevity. Dev Cell. 2021;56(10):1394–407. https://doi.org/10.1016/j.devcel.2021.03.034.
64. Carnamucio F, Abate C, Cordaro M, Foti C, Donato S, Saija F, et al. Comprehensive speciation and computational study of Cu2+ and Zn2+ complexation with O-Phosphorylethanolamine and O-Phosphorylcholine in aqueous solution. Molecules. 2025;30(19):3923. https://doi.org/10.3390/molecules30193923.
65. Zappelli E, Daniele S, Ceccarelli L, Vergassola M, Ragni L, Mangano G, et al. α-Glyceryl-phosphorylethanolamine protects human hippocampal neurons from ageing-induced cellular alterations. Eur J Neurosci. 2022;56(5):4514–28. https://doi.org/10.1111/ejn.15783.
66. Dawaliby R, Trubbia C, Delporte C, Noyon C, Ruysschaert JM, Van Antwerpen P, et al. Phosphatidylethanolamine is a key regulator of membrane fluidity in eukaryotic cells. J Biol Chem. 2016;291(7):3658–67. https://doi.org/10.1074/jbc.M115.706523.
67. Ballweg S, Sezgin E, Doktorova M, Covino R, Reinhard J, Wunnicke D, et al. Regulation of lipid saturation without sensing membrane fluidity. Nat Commun. 2020;11(1):756. https://doi.org/10.1038/s41467-020-14528-1.
68. Amargant F, Manuel SL, Tu Q, Parkes WS, Rivas F, et al. Ovarian stiffness increases with age in the mammalian ovary and depends on collagen and hyaluronan matrices. Aging Cell. 2020;19(11):e13259. https://doi.org/10.1111/acel.13259.
69. Maines LW, Keller SN, Smith RA, Smith CD. Opaganib promotes weight loss and suppresses high-fat diet-induced obesity and glucose intolerance. Diabetes Metab Syndr Obes. 2025;18:969–83. https://doi.org/10.2147/DMSO.S514548.
70. Wu R, Yu H, Xu J, Tan Z, Lan Y, Shi D. Effects of acute low intensity aerobics and blueberry juice on arterial stiffness in young adults. NPJ Sci Food. 2025;9(1):47. https://doi.org/10.1038/s41538-025-00408-9.
71. Naderi J, Johnson AK, Thakkar H, Chandravanshi B, Ksiazek A, et al. Ceramide-induced FGF13 impairs systemic metabolic health. Cell Metab. 2025. https://doi.org/10.1016/j.cmet.2025.03.002.
72. Xu L, Wu J, Tian J, Zhang B, Zhao Y, Zhao Z, et al. Machine learning unveils sphingolipid metabolism's role in tumour microenvironment and immunotherapy in lung

cancer. J Cell Mol Med. 2025;29(7):e70435. https://doi.org/10.1111/jcmm.70435.
73. Janneh AH, Kassir MF, Atilgan FC, Lee HG, Sheridan M, et al. Crosstalk between pro-survival sphingolipid metabolism and complement signaling induces inflammasome-mediated tumor metastasis. Cell Rep. 2022;41(10):111742. https://doi.org/10.1016/j.celrep.2022.111742.
74. Janneh AH, Ogretmen B. Targeting sphingolipid metabolism as a therapeutic strategy in cancer treatment. Cancers (Basel). 2022;14(9):2183. https://doi.org/10.3390/cancers14092183.
75. Chitkara S, Atilla-Gokcumen GE. Decoding ceramide function: how localization shapes cellular fate and how to study it. Trends Biochem Sci. 2025;50(4):356–67. https://doi.org/10.1016/j.tibs.2025.01.007.
76. Shen X, Feng R, Zhou R, Zhang Z, Liu K, Wang S. Ceramide as a promising tool for diagnosis and treatment of clinical diseases: a review of recent advances. Metabolites. 2025;15(3):195. https://doi.org/10.3390/metabo15030195.
77. Crivelli SM, Quadri Z, Elsherbini A, Vekaria HJ, Sullivan PG, Zhi W, et al. Abnormal regulation of mitochondrial sphingolipids during aging and Alzheimer's disease. ASN Neuro. 2024;16(1):2404367. https://doi.org/10.1080/17590914.2024.2404367.
78. Xu A, Liu Y, Wang B, Zhang Q, Ma Y, Xue Y, et al. Ceramide synthase 6 induces mitochondrial dysfunction and apoptosis in hemin-treated neurons by impairing mitophagy through interacting with sequestosome 1. Free Radic Biol Med. 2025;227:282–95. https://doi.org/10.1016/j.freeradbiomed.2024.12.018.
79. van der Reest J, Nardini Cecchino G, Haigis MC, Kordowitzki P. Mitochondria: their relevance during oocyte ageing. Ageing Res Rev. 2021;70:101378. https://doi.org/10.1016/j.arr.2021.101378.
80. Zhang C, Zhao M, Xue Y, Tang X, Shi D, Wang X. Effects of vitrification on mitochondrial ultrastructure and membrane potential and its distribution in mouse oocytes. Cryo Letters. 2024;45(5):301–8.
81. Wang W, Liu H, Liu S, Hao T, Wei Y, Wei H, et al. Oocyte-specific deletion of eukaryotic translation initiation factor 5 causes apoptosis of mouse oocytes within the early-growing follicles by mitochondrial fission defect-reactive oxygen species-DNA damage. Clin Transl Med. 2024;14(8):e1791. https://doi.org/10.1002/ctm2.1791.
82. Salmonowicz H, Szczepanowska K. The fate of mitochondrial respiratory complexes in aging. Trends Cell Biol. 2025. https://doi.org/10.1016/j.tcb.2025.02.008.
83. Fitzpatrick FM, Kory N. Guardians of the cell: mitochondria as a rheostat for cellular NAD+ levels. Nat Metab. 2024;6(12):2215–7. https://doi.org/10.1038/s42255-024-01160-2.
84. Nasuhidehnavi A, Zarzycka W, Górecki I, Chiao YA, Lee CF. Emerging interactions between mitochondria and NAD+ metabolism in cardiometabolic diseases. Trends Endocrinol Metab. 2025;36(2):176–90. https://doi.org/10.1016/j.tem.2024.07.010.
85. da Fonseca Junior AM, Ispada J, Dos Santos EC, de Lima CB, da Silva JVA, Paulson E, et al. Adaptative response to changes in pyruvate metabolism on the epigenetic landscapes and transcriptomics of bovine embryos. Sci Rep. 2023;13(1):11504. https://doi.org/10.1038/s41598-023-38686-6.
86. Bao S, Yin T, Liu S. Ovarian aging: energy metabolism of oocytes. J Ovarian Res. 2024;17(1):118. https://doi.org/10.1186/s13048-024-01427-y.
87. Collado-Fernandez E, Picton HM, Dumollard R. Metabolism throughout follicle and oocyte development in mammals. Int J Dev Biol. 2012;56(10–12):799–808. https://doi.org/10.1387/ijdb.120140ec.
88. Harris SE, Leese HJ, Gosden RG, Picton HM. Pyruvate and oxygen consumption throughout the growth and development of murine oocytes. Mol Reprod Dev. 2009;76(3):231–8. https://doi.org/10.1002/mrd.20945.
89. Xie HL, Wang YB, Jiao GZ, Kong DL, Li Q, Li H, et al. Effects of glucose metabolism during in vitro maturation on cytoplasmic maturation of mouse oocytes. Sci Rep. 2016;6:20764. https://doi.org/10.1038/srep20764.
90. Ilyas A, Wijayasinghe YS, Khan I, Park YS. Implications of trimethylamine N-oxide and betaine in human health: beyond being osmoprotective compounds. Biomolecules. 2022;12:1485.
91. Zawieja E, Chmurzyńska A. Betaine and aging: a narrative review of findings, possible mechanisms, research perspectives, and practical recommendations. Pharmacol Rep. 2024;76:280–92.
92. Chen S, He T, Chen J, Wang Y. Betaine delays age-related muscle loss by mitigating Mss51-induced impairment in mitochondrial respiration via Yin Yang 1. J Cachexia Sarcopenia Muscle. 2024;15:788–800.
93. Geng L, Ping J, Wu RH, Yang H. Systematic profiling reveals betaine as an exercise mimetic for geroprotection. Cell. 2025;188:2707-2722.e22.
94. Zhang Y, Liu X, Wang Y. Betaine: a comprehensive review on dietary sources, health benefits, mechanisms of action, and application. Front Med. 2025;19:689–90.
95. Johnson AR, Lao S, Wang T, Galanko JA, Zeisel SH. Choline dehydrogenase polymorphism rs12676 is a functional variation and is associated with changes in human sperm cell function. PLoS ONE. 2012;7(4):e36047. https://doi.org/10.1371/journal.pone.0036047.
96. Zhang D, Jing H, Dou C, Zhang L, Wu X, Wu Q, et al. Supplement of betaine into embryo culture medium can rescue injury effect of ethanol on mouse embryo development. Sci Rep. 2018;8(1):1761. https://doi.org/10.1038/s41598-018-20175-w.
97. Catalán J, Martínez-Rodero I, Yánez-Ortiz I, Mateo-Otero Y, Bragulat AF, Nolis P, et al. Metabolic profiling of preovulatory follicular fluid in jennies. Res Vet Sci. 2022;153:127–36. https://doi.org/10.1016/j.rvsc.2022.10.026.
98. Attia YA, El-Naggar AS, Abou-Shehema BM, Abdella AA. Effect of supplementation with trimethylglycine (betaine) and/or vitamins on semen quality, fertility, antioxidant status, DNA repair and welfare of roosters exposed to chronic heat stress. Animals. 2019;9(8):547. https://doi.org/10.3390/ani9080547.

99. Sfakianoudis K, Zikopoulos A, Grigoriadis S, Seretis N, Maziotis E, Anifandis G, et al. The role of one-carbon metabolism and methyl donors in medically assisted reproduction: a narrative review of the literature. Int J Mol Sci. 2024;25(9):4977. https://doi.org/10.3390/ijms25094977.
100. Dabaja MZ, Dos Santos AA, Christofolini DM, Barbosa CP, de Oliveira DN, de Oliveira AN, et al. Comparative metabolomic profiling of women undergoing in vitro fertilization procedures reveals potential infertility-related biomarkers in follicular fluid. Sci Rep. 2022;12(1):20531. https://doi.org/10.1038/s41598-022-24775-5.